Shell-model description of $N \simeq Z$ $1f_{7/2}$ nuclei

F. Brandolini and C. A. Ur*
Dipartimento di Fisica dell'Università and INFN Sezione di Padova, I–35131 Padova, Italy
(Received 3 December 2004; published 26 May 2005)

The available spectroscopic data for nuclei middle and second half of the $1f_{7/2}$ shell are well reproduced by shell-model calculations. For natural parity states of several odd-*A* nuclei, a comparison of shell-model calculations in the full *pf* configuration space with the Nilsson diagram and particle-rotor predictions shows that prolate strong coupling applies at low excitation energy. Multiquasiparticle rotational bands and, in some cases, band crossings have been revealed. Coriolis decoupling effects are observed only in nuclei at the beginning of the shell. The ground state bands experience a change from a collective to a noncollective regime, approaching the termination in the $1f_{7/2}^n$ space. Similar features are observed in the even-even $N = Z$ nuclei ^{48}Cr and ^{52}Fe and $N = Z + 2$ nuclei ^{46}Ti and ^{50}Cr. Evidence of the vibrational γ band is discussed in the $N = Z$ nuclei. A brief review is also presented for unnatural parity levels.

DOI: 10.1103/PhysRevC.71.054316 PACS number(s): 21.10.−k, 21.60.Cs, 23.40.−s, 27.40.+z

I. INTRODUCTION

During the last decade, extensive theoretical work has been conducted to improve the quality of the shell-model (SM) description of the $1f_{7/2}$ nuclei, with particular care taken to understand the origin of their rotational collectivity [1]. The first nuclei studied in detail were ^{48}Cr [2] and ^{50}Cr [3]. The next step was the study of several odd-*A* nuclei, particularly the mirror pair ^{49}Cr-^{49}Mn, for which the connection with the particle rotor model (PRM) was pointed out [4].

These theoretical advances were accompanied by parallel experimental work at the National Laboratories of Legnaro (LNL), which exploited the advantages of the large γ-detector array GASP. The level schemes of ^{48}Cr and ^{50}Cr have been enriched [5,6], and the understanding of their collective properties has been greatly increased with the help of lifetime measurements [7]. The research was thereafter extended to several nuclei in the middle of $1f_{7/2}$, where attention was focused on the yrast sequence of levels up to the smooth band termination in the $1f_{7/2}^n$ and $1d_{3/2}^{-1} \otimes 1f_{7/2}^{n+1}$ configuration spaces, for natural parity and unnatural parity, respectively. These structures were efficiently populated in heavy-ion-induced fusion reactions. SM calculations in the full *pf* configuration space [1] reproduce very well the excitation energies of the observed natural parity levels, as well as the $B(E2)$ and $B(M1)$ rates. The double shell closure at ^{56}Ni is weak enough to allow large mixing to occur with with the other orbitals of the *pf* configuration space, giving rise to collective effects which could hardly be imagined to occur in this nuclear region; but the closure is also strong enough to produce clear smooth terminations in the low-lying bands of $1f_{7/2}$ nuclei.

In general, low-lying levels can be classified in the framework of the prolate Nilsson diagram. A band crossing along the ground state (gs) band was first recognized in ^{50}Cr, as being caused by the four-quasiparticle (4-qp) $K^\pi = 10^+$ band, originated by the simultaneous excitations of a proton from the $[321]3/2^-$ to the $[312]5/2^-$ orbital and of a neutron from the $[312]5/2^-$ to the $[303]7/2^-$ orbital [8]. Its head is the yrast level 10^+, which gives rise to the observed backbending. This interpretation was confirmed in a recent paper, where evidence of the two 2-qp bands with $K^\pi = 4^+$ for protons and $K^\pi = 6^+$ for neutrons was found [9] and where it was shown that deformation alignment (strong coupling) can explain the observed mirror energy differences [10], mainly due to Coulomb energy differences (CED).

SM [2], cranked Hartree-Fock-Bogoliubov (CHFB) [2,11], and cranked Nilsson-Strutinsky (CNS) [12] calculations do not confirm that the backbending at $I^\pi = 12^+$ in ^{48}Cr is due to a band crossing, as inferred by projected shell-model (PSM) calculations [13]. Rather, it has been related to the smooth termination in a $v = 4$ seniority subspace [8], as suggested by the calculations of Ref. [14].

In ^{49}Cr, the backbending of the $K^\pi = 5/2^-$ gs band at $19/2^-$ was similarly interpreted as the termination in a $v = 3$ subspace [8]. The level at 3528 keV was identified as the head of a 3-qp $K^\pi = 13/2^-$ band, which is described as due to the excitation of a proton from the $[321]3/2^-$ to the $[312]5/2^-$ orbital followed by the coupling to the maximum *K* value of all unpaired nucleons [15,16]. Recently, two more members of this band were observed, as well as states belonging to the 1-qp bands based on the Nilsson orbitals $[321]1/2^-$, $[303]7/2^-$, and $[321]3/2^-$ [18].

Very interesting features were observed also for the positive parity levels of ^{49}Cr. Above the 1-qp $K^\pi = 3/2^+$ band built on the $[202]3/2^+$ orbital, a 3-qp $K^\pi = 13/2^+$ band becomes yrast and acts to trap the decay flux toward positive parity levels of the $K^\pi = 3/2^+$ band. The 3-qp band is described as being due to the excitation of a proton from the $[202]3/2^+$ orbital to the empty $[312]5/2^-$ one, followed by the coupling to the maximum *K* of the three unpaired nucleons [15] or, in a different representation, as a $\pi d_{3/2}^{-1} \otimes {}^{50}\mathrm{Mn}(I = 5, T = 0)$ configuration.

In this work, we shall mainly discuss natural parity bands in several $N \simeq Z$ odd-*A* and even-even nuclei, pointing out further evidence, (not considered in detail in recent reviews [19,20]) of smooth terminations, multi-qp bands, band crossings, and the noncollective rotational regime, complementing the

*On leave from NIPNE, Bucharest, Romania.

pioneering work of Ref. [4]. The SM-calculated static electromagnetic (em) moments will provide a powerful tool for understanding the underlying structure. These values have, in fact, to be considered reliable because of the good agreement achieved for level schemes, as well as $B(E2)$ and $B(M1)$ values, in most discussed nuclei and in particular in ^{48}Cr, ^{50}Cr, and ^{49}Cr, [7,9,15,16], which are discussed here.

For reasons of clarity, the comparison will be restricted to levels up to the termination in the $1f_{7/2}^n$ configuration space even if good agreement has been found beyond that point [20]. For the same reason, odd-odd nuclei will not be discussed in spite of the excellent agreement achieved [21,22].

II. ABOUT SHELL-MODEL CALCULATIONS

SM calculations will be compared with experimental level schemes taken from the last review in Nuclear Data Sheets (NDS) and most recent references.

Calculations for the natural parity levels have been previously made in the full *pf* shell using the realistic effective interactions KB3 [1], KB3G [20], FPD6 [23], and KLS [24]. The KB3G interaction is just a slight modification of KB3 to better reproduce the nuclear properties approaching ^{56}Ni. Generally, their results are rather similar, but in particular cases some give better predictions. For instance, in proximity of ^{48}Cr the KB3/KB3G interaction gives excellent predictions while FPD6 is about 10% too strong. Recently, the GXPF1 interaction has been proposed for *pf* nuclei, which was obtained by fitting four single-particle energies and 195 two-body matrix elements. This interaction is somewhat better than KB3G for nuclei around and above ^{56}Ni [25,26]. The KB3G interaction was adopted in the present calculations because it reproduces somewhat better the energies for most of the nuclei considered here.

A realistic interaction is made of a monopole and a multipole part. The latter, which contains most of the structural information, has been shown to be dominated by the pairing and quadrupole terms [28]. Calculations with a schematic interaction pairing plus quadrupole ($P + QQ$) are currently made, since it has been shown that it can simulate realistic interactions well [27].

Present calculations were made assuming isospin conservation, i.e., neglecting the effect of Coulomb interaction, for the lowest isospin value. Bare nucleon g-factor values and effective charges (1.5 for protons and 0.5 for neutrons) were adopted. Standard personal computers with Pentium 4 CPU's and 2 GB RAM were used. The SM code ANTOINE was used in its Internet-distributed version [29,30].

When truncation was necessary, a limited number of nucleons s were moved from the $1f_{7/2}2p_{3/2}$ subspace to the $1f_{5/2}$ and $2p_{1/2}$ orbitals. Space truncation was made for $A \geqslant 52$. This truncation differs somewhat from the one commonly adopted, which counts all the particles outside the $f_{7/2}$ orbital. Some remarks on the consequences of configuration space truncation are worth mentioning here. It was observed that most of the rotational collectivity is already reproduced in a $1f_{7/2}2p_{3/2}$ subspace, where a "quasi SU(3)" scheme is valid [31]. This means that the quadrupole deformation originates in a rather similar way as in the SU(3) scheme, which applies to the *sd* shell. From an empirical point of view, the main consequences of using the reduced space are that the deformation is slightly reduced and the binding energies of the lower levels are smaller.

III. COMPARISON OF SM AND ROTOR ESTIMATES

The SM results for em moments will be compared with the predictions of the axial rotor [32], where the configuration is described by the Nilsson diagram. The intrinsic electric quadrupole moment $Q_\circ$ is derived from the calculated spectroscopic quadrupole moment Q_s according to the formula

$$Q_s = Q_\circ \frac{3K^2 - I(I+1)}{(I+1)(2I+3)}. \quad (1)$$

The intrinsic quadrupole moment can also be derived from the $B(E2)$ values using the formula

$$B(E2) = \frac{5}{16\pi} Q_t^2 \langle I_i K 20 | I_f K \rangle^2, \quad (2)$$

where it is denoted as Q_t.

In the following we will assume $Q_t = Q_\circ$. Its relation with the deformation parameter β is given by the equation [33]

$$Q_\circ = 1.09 Z A^{2/3} \beta (1 + 0.36\beta) \quad e\,\mathrm{fm}^2. \quad (3)$$

For further use, we define the parameter $\beta^* = \beta(1 + 0.36\beta)$, because in the literature some authors adopt the coefficient 0.16 for β inside the brackets.

Concerning the magnetic properties of odd-A nuclei, the g-factor values are expressed as

$$g = g_R + (g_K - g_R)\frac{K^2}{I(I+1)}, \quad (4)$$

and the $M1$ reduced probabilities are

$$B(M1) = \frac{3}{4\pi} \langle I_i K 10 | I_f K \rangle^2 \times (g_K - g_R)^2 K^2 \mu_N^2 \qquad (for\ K \neq 1/2). \quad (5)$$

A decoupling term must be added to Eq. (5) when $K = 1/2$. These formulas have to be considered as qualitative since, even in the extreme hypothesis of no residual interaction, K values are mixed by the Coriolis force. This is accounted for by PRM [34]; but it will be shown that generally the mixing caused by the Coriolis force is not large in the second half of the $1f_{7/2}$ shell, so the calculations provide an adequate reference. It is necessary to use PRM in the first half of the shell, where the $[330]1/2^-$ Nilsson orbital is important and thus the Coriolis force gives rise to a partial Coriolis decoupling (CD).

Equations (1) and (2) will be applied to even-even nuclei as well. The magnetic properties of the $N = Z$ nuclei ^{48}Cr and ^{52}Fe will not be considered here because they are only slightly sensitive to the nuclear structure. In self-conjugated nuclei, the g-factor values approach closely the isoscalar value $\frac{g_p + g_n}{2}$, where the nucleon g factors are the Schmidt values in the $1f_{7/2}$ shell, while $B(M1)$ values are very small. On the other hand, the magnetic properties of $N = Z + 2$ nuclei do not have a simple interpretation.

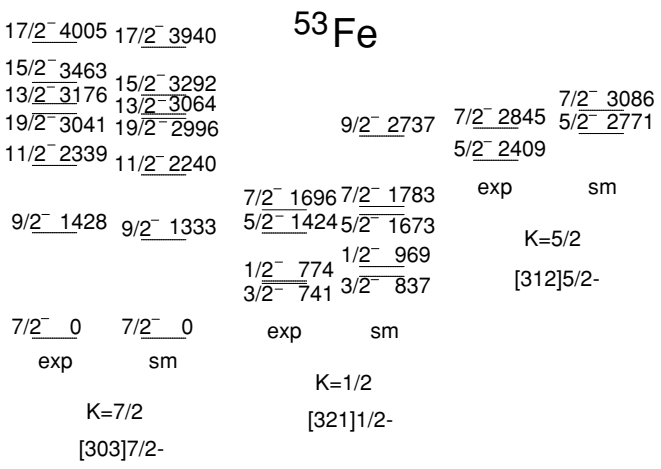

FIG. 1. Comparison of experimental negative parity levels in ^{53}Fe with SM predictions ($s = 3$).

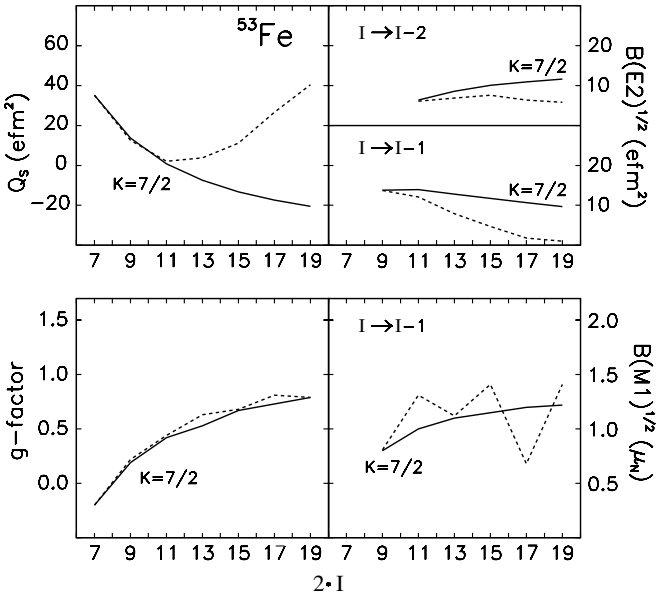

FIG. 2. Calculated em moments in the gs band of ^{53}Fe. Rotor ($\beta^* = 0.19$), solid lines; SM, dashed lines.

K mixings of the order of 10% are often estimated, usually larger in the full pf configuration space than in the restricted $f_{7/2}p_{3/2}$ one. This makes the observation of intraband transitions difficult, because they are unfavored by the low transition energy, and it may perturb the values of em moments but, hopefully, without obscuring the basic structural effects. Mixing increases with spin because of both the decrease in the deformation and the higher level density.

The 1-qp sidebands will not be discussed in detail, since experimental data are often not precise. The Nilsson orbital assignments in the displayed level schemes are in general tentative.

A. ^{53}Fe and ^{43}Sc

For the present scope, it is important to examine in detail the gs band of the nucleus ^{53}Fe, whose terminating state ($I^\pi = 19/2^-$, $E_x = 3049$ keV, $\tau = 3.6$ min) is dominated by a $\pi f_{7/2}^{-2}(I = 6) \otimes \nu f_{7/2}^{-1}$ configuration and is an yrast trap, as it lies 400 keV below the yrast $15/2^-$ state. Its experimental level scheme is compared with the SM-predicted one in Fig. 1, where an $s = 3$ truncation was adopted. Experimental data were taken from NDS and a recent paper [35]. Experimental $B(E2)$ and $B(M1)$ values along the gs band are only known for the $9/2^-$ and the $11/2^-$ levels, with a poor precision. SM predictions are consistent inside the large error bar. Two 1-qp sidebands are tentatively assigned. The largest contribution to the wave function of the yrast $1/2^-$ and $3/2^-$ levels comes from the excitation of one neutron to the $2p_{3/2}$ orbital, as expected in the case of the $[321]1/2^-$ orbital. Deformation at low spin is also revealed by the observed fast $E2$ (31 W.u.) transition from $5/2^-$ to $1/2^-$, which belongs to the $K = 1/2$ sideband.

^{53}Fe is a very convenient testing bench to investigate how rotational collectivity builds up. In the second half of the $1f_{7/2}$ shell, there is no disturbance from two- and four-hole configurations, which are effective at the beginning of the shell [36]; moreover, the $2p_{3/2}$ orbital is very active in generating deformation.

All calculated em observables for states of ^{53}Fe belonging to the gs band are reported in Fig. 2, where SM predictions are compared with the ones for a prolate rotor. Done differently than in Ref. [4], Q_s rather than $Q_\circ$ is plotted since it will be shown that Eq. (1) cannot be applied in general. Furthermore, the square roots of the $B(E2)$ values are reported because they are approximately linearly proportional to the deformation as the Q_s values are. The Q_s value of the gs state is predicted to be large and positive, as expected for a prolate $K = 7/2$ band with $\beta^* \simeq 0.19$. Calculated Q_s and $B(E2)$ values agree with rotor predictions only at low spins up to 11/2, so that the typical $I(I + 1)$ energy appearance has no room to become evident. What occurs above 11/2 will be discussed later.

The level scheme for the $\pi^{-2}\nu^{-1}$ ^{53}Fe is substantially different from that of its cross conjugate $\pi^1\nu^2$ ^{43}Sc; while in the $1f_{7/2}^n$ space, cross-conjugate nuclei should have identical level schemes, pointing to different configuration mixing and collective properties. Both ^{43}Sc and ^{53}Fe, as in general $1f_{7/2}$ nuclei, are described at low energy with a prolate shape. In both cases, the gs level is $7/2^-$, but in ^{43}Sc a large signature splitting (SS) is observed. Another striking difference is that the predicted $B(E2)$ values of the transition from the yrast level $9/2^-$ to the $7/2^-$ in ^{43}Sc and ^{53}Fe are 13.6 and 217.2 $e\,\mathrm{fm}^2$, respectively. The latter is a fingerprint of rotational collectivity in ^{53}Fe, since in a $1f_{7/2}^{-3}$ space only one third of this value is predicted. The properties of ^{43}Sc, on the other hand, can be roughly described by PRM predictions, assuming a slightly prolate shape with $\beta^* = 0.10$, which predict rotational alignment in the gs band built on the $[330]1/2^-$ Nilsson orbital. SM predictions are compared with PRM ones in Table I. There is some correspondence, in spite of the naive description. It has to be remarked that SM calculations are not very good for ^{43}Sc, because two- and four-hole configurations strongly mix at low spin in nuclei close to ^{40}Ca [36]. This does not

TABLE I. Comparison of ^{43}Sc properties with SM and PRM predictions.

I	E_x (keV)	$E_{\rm sm}$ (keV)	Q_s (e fm^2)	$B(E2, \Delta I = 1)$ (e^2 fm^4)	$B(E2, \Delta I = 2)$ (e^2 fm^4)	$E_{\rm prm}$ (keV)	Q_s (e fm^2)	$B(E2, \Delta I = 1)$ (e^2 fm^4)	$B(E2, \Delta I = 2)$ (e^2 fm^4)
$7/2^-$	0	0	−18	–	–	0	−8	–	–
$9/2^-$	1883	1999	−11	14	–	1905	−27	14	–
$11/2^-$	1830	1816	−17	16	26	1570	−13	8	27
$13/2^-$	3958[a]	3445	−10	5	13	5364	−9	8	32

[a] Ref. [37]

occur in the isotope ^{47}Sc with $\pi^1\nu^{-2}$, where good agreement is achieved by SM [4].

The different structure of the cross-conjugate nuclei is confirmed by the contribution of the $1f_{7/2}^n$ configuration (expressed in percentage) to the states along the gs band. For the levels with spin 7/2, 9/2, 11/2, 13/2, 15/2, 17/2, and 19/2, the contributions are 79, 96, 72, 95, 78, 88, and 96 in ^{43}Sc and 56, 54, 58, 60, 63, 60, and 64 in ^{53}Fe. The staggering of the values in ^{43}Sc is related to the SS caused by CD, where the $7/2^-$ ground state has the favored signature. These numbers provide, moreover, a qualitative explanation for the inversion between the $15/2^-$ and $19/2^-$ observed in ^{53}Fe. The level scheme calculated in the $1f_{7/2}^{\pm3}$ space predicts the inversion, as a consequence of the very attractive $V_{pn}(I = 7, T = 0)$ term. The inversion is preserved in ^{53}Fe because the contribution of the $1f_{7/2}^{-3}$ component is similar in the two states; whereas in ^{43}Sc, the $1f_{7/2}^{3}$ contribution is about 20% larger for the $19/2^-$, so the $15/2^-$ has an additional binding energy that lowers it below the $19/2^-$ level. More than one third of the upper orbital occupation refers to the $2p_{3/2}$ one, which gives rise to large quadrupole terms.

CD is expected to be large at low spin if the gs band is based on the $[330]1/2^-$ orbital (as in ^{43}Sc); it is noticeable for the $[321]3/2^-$ orbital and small for the $[312]5/2^-$ and $[303]7/2^-$ orbitals. It becomes again important in the case of the intruder orbital $[440]1/2^+$, originating from the $1g_{9/2}$ orbital.

As shown in Fig. 2, the Q_s values of the ^{53}Fe gs band start to increase above $I^\pi = 11/2^-$, reaching at the terminating spin $19/2^-$ a maximum of 42.9 e fm^2, calculated with $s = 4$ (it may be a little larger in full *pf* calculations). This is consistent with its holelike nature, to which a prolate noncollective shape pertains. In a semiclassical description, $Q_s = Q_\circ$ and thus $\beta^* \simeq 0.11$ is derived from Eq. (3). Since $Q_s = 25$ e fm^2 is predicted in the $1f_{7/2}^n$ space, one infers that the terminating state is strongly polarized by the upper orbitals, which contribute by about 40%, getting a strong enhancement of the noncollective prolateness. Its Q_s value is stable upon large variations of the orbital binding energies, and its measurement would be of great interest. Its terminating nature is confirmed by the fact that yrast $21/2^-$ and $23/2^-$ levels are predicted more than 4 MeV above it.

A further test is the comparison of SM predictions with the experimental $B(E4)$ value of 638(130) e^2 fm^6 for the transition connecting the terminating level $19/2^-$ to the $11/2^-$ level. Using $s = 6$ and bare nucleon electric charges, the values are 1106, 756, and 137 e^2 fm^6, for the interactions KB3G, GXPF1, and FPD6, respectively. The KB3G estimate is somewhat too large and the FPD6 one too small. Only a few $B(E4)$ values are, however, known with sufficient precision in this region to draw a general conclusion.

The shape evolution from a collective rotation to a noncollective one approaching termination is commonly described with the configuration-dependent CNS model [38], as recently made for ^{50}Mn, where the low-lying bands terminate as prolate noncollective, similar to those in ^{53}Fe [39]. In a β-γ plane, the shape changes from $\gamma \simeq 0$ at the bottom of the gs band to $\gamma \simeq -120$ at its termination (Lund convention), as qualitatively depicted in Fig. 3.

One may, however, question whether a mean-field description such as the CNS one can describe accurately a system with few valence particles or holes. One should find that in a few steps the nucleus changes in sequence to the triaxial collective, oblate collective, and finally prolate noncollective shapes. It seems more realistic to imagine a direct change from prolate collective to prolate noncollective, because an oblate collective shape is likely inhibited by the simple shell-model structure. It is known that the single-particle structure of a prolate nucleus may favor a prolate noncollective shape [40]. More arguments

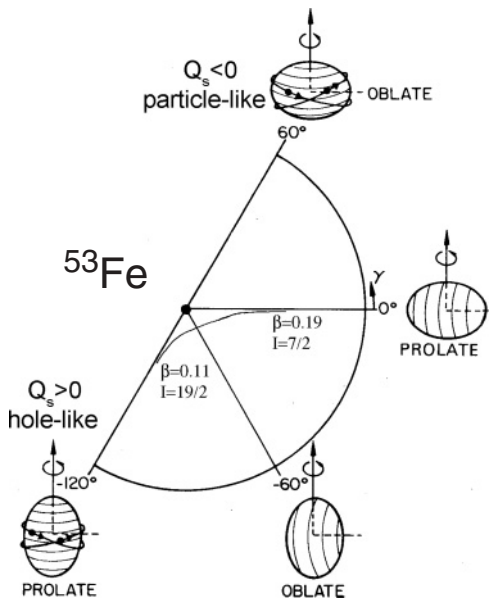

FIG. 3. Schematic representation of the shape evolution along the gs band in ^{53}Fe.

TABLE II. Q_s and g-factor values of terminating states.

Nuclide	Config.	I^π	$P(f_{7/2}^n)$ (%)	Q_s (e fm^2)	$Q_s(f_{7/2}^n)$ (e fm^2)	$g_{\rm SM}$	$g_{\rm emp}$
^{55}Co	π^{-1}	$7/2^-$	62.6	24.1	17.5	1.350	1.38
^{55}Ni	ν^{-1}	$7/2^-$	"	14.8	5.8	−0.271	−0.30
^{54}Fe	π^{-2}	6^+	61.1	27.2	19.8	1.337	1.38
^{54}Ni	ν^{-2}	6^+	"	18.9	6.6	−0.256	−0.30
^{53}Fe	$\pi^{-2}\nu^{-1}$	$19/2^-$	60.7	42.9	25.5	0.770	0.80
^{53}Co	$\pi^{-1}\nu^{-2}$	$19/2^-$	"	43.1	23.8	0.318	0.28
^{52}Fe	$\pi^{-2}\nu^{-2}$	12^+	60.9	47.1	26.1	0.547	0.54
^{51}Mn	$\pi^{-3}\nu^{-2}$	$27/2^-$	68.4	32.7	18.6	0.646	0.65
^{51}Fe	$\pi^{-2}\nu^{-3}$	$27/2^-$	"	39.4	23.5	0.446	0.43
^{50}Cr	$\pi^{-4}\nu^{-2}$	14^+	75.3	7.1	6.4	0.668	0.68
^{50}Fe	$\pi^{-2}\nu^{-4}$	14^+	"	22.3	19.3	0.421	0.40
^{49}Cr	$\pi^{-4}\nu^{-3}$	$31/2^-$	88.9	1.6	4.0	0.586	0.57
^{49}Mn	$\pi^{-3}\nu^{-4}$	$31/2^-$	"	9.8	12.0	0.503	0.51
^{48}Cr	$\pi^4\nu^4$	16^+	89.4	−6.7	0	0.553	0.54
^{47}V	$\pi^3\nu^4$	$31/2^-$	87.5	−19.2	−12.0	0.534	0.51
^{47}Cr	$\pi^4\nu^3$	$31/2^-$	"	−14.4	−4.0	0.549	0.57
^{46}Ti	$\pi^2\nu^4$	14^+	86.7	−24.2	−19.3	0.449	0.40
^{46}Cr	$\pi^4\nu^2$	14^+	"	−18.8	−6.4	0.638	0.68
^{45}Ti	$\pi^2\nu^3$	$27/2^-$	90.0	−26.8	−23.5	0.471	0.43
^{45}V	$\pi^3\nu^2$	$27/2^-$	"	−25.8	−18.6	0.616	0.65
^{44}Ti	$\pi^2\nu^2$	12^+	94.3	−27.7	−26.1	0.545	0.54
^{43}Sc	$\pi^1\nu^2$	$19/2^-$	96.1	−23.1	−23.8	0.330	0.28
^{43}Ti	$\pi^2\nu^1$	$19/2^-$	"	−26.3	−25.5	0.765	0.80

for a shape change will be presented in the discussion of other nuclei.

The evolution of Q_s values approaching the terminating spin $19/2^-$ is incompatible with rotational alignment, as proposed elsewhere for nuclei of this region [41], because a negative value of Q_s would be expected in that case, as one has to give I a large value and K a small one in Eq. (1).

In the past, the noncollective rotation of the prolate shape at the band termination was alternatively interpreted as a high-K collective prolate rotation [42]. This misunderstanding originated from the large overlap of the two wave functions. In fact, an $I = K = 19/2$ state is oriented spatially almost in the same manner, where $Q_s = 0.74\ Q_\circ$, according to Eq. (1). The substantial physical difference is that the nonrotational state is a terminating one, while the hypothetical $K = 19/2$ state would be a bandhead. The latter description is clearly excluded by the observation that Q_s increases gradually with the level spin approaching termination.

The prevalence of the three-hole configuration approaching the termination reflects the prediction of increasing CED values, as observed [35]. In fact, it is known that the wave functions of two identical nucleons in identical orbitals get a minimum spatial overlap with increasing spin, leading to a lower Coulomb energy and a larger binding energy for ^{53}Fe, where a proton pair aligns, with respect to its mirror ^{53}Co.

The KB3G predictions of Q_s values for several terminating states in $N \simeq Z$ nuclei are compared with $1f_{7/2}^n$ predictions in Table II. Calculations were made in the full pf configuration space, except for $A = 53$, 54 and $A = 55$ where $s = 6$ and $s = 3$ truncations were assumed, respectively (obviously, a four-hole configuration coincides with a four-particle one). These states are generally supposed to have a nearly pure $1f_{7/2}^n$ configuration, but this turns out to be not true approaching the end of the shell, as shown in the fourth column of Table II, where the percentages of $1f_{7/2}^n$ configuration are reported. Calculations made with the GXPF1 interaction are nearly equivalent for ^{53}Fe, while the FPD6 one would predict a mixing about 30% higher for the terminating states approaching shell closure, accompanied by up to 20% larger $B(E2)$ rates.

One further observes that a negative value of Q_s is calculated for ^{48}Cr, where 0 is expected in the $1f_{7/2}$ space. Similarly, a negative offset applies to neighboring nuclei. The scale factor of Q_s for the single proton-hole nucleus ^{55}Co in the $1f_{7/2}^n$ space is $(2j-1)/(2j+1)\langle r^2\rangle$ [32]. It is peculiar that $\nu^{-2}\pi^{-1}$ and $\nu^{-1}\pi^{-2}$ configurations have a similar Q_s value.

The experimental g-factor value of the $19/2^-$ level in ^{43}Sc is known to be 0.329(1), that of the 6^+ level in ^{54}Fe is 1.37(3), and finally the g-factor of the single-hole $7/2^-$ level in ^{55}Co is 1.378(1). Thus, all experimental values known with high precision agree with the SM predictions of Table II.

A critical point is the capability of the effective interaction to get good results in proximity of the shell closure. The experimental value $B(E2, 6^+ \rightarrow 4^+) = 39.7(5)\ e\,\text{fm}^2$ in ^{54}Fe provides an test for the effective interactions. The interactions KB3G, GXPF1, and FPD6 give $B(E2, 6^+ \rightarrow 4^+)$ values 40.3, 40.7, and 46.7 e fm^2, respectively, using an $s = 4$ truncation. It turns out that the FPD6 interaction overestimates the $B(E2)$ value by about 20%. The $1f_{7/2}^n$ prediction is 23.1 e fm^2, independent from the adopted interaction.

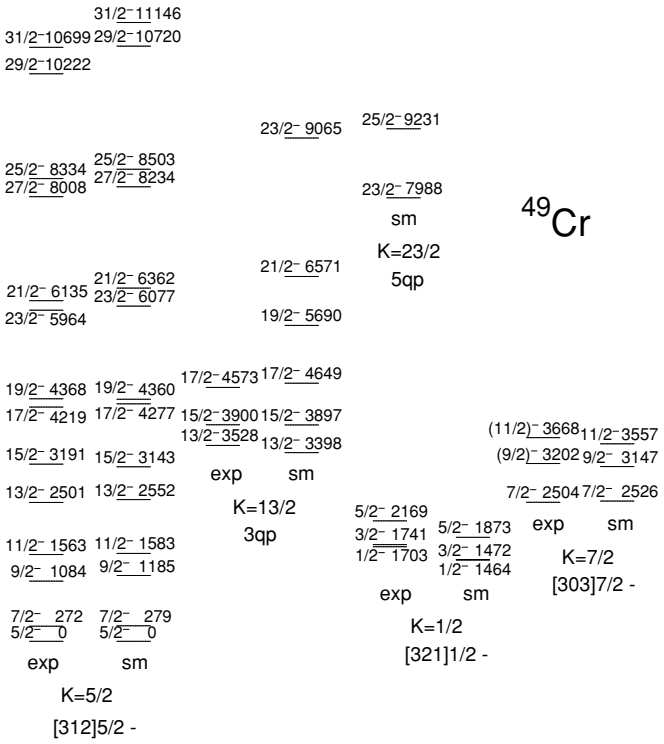

FIG. 4. Comparison of experimental negative parity levels in ^{49}Cr with SM predictions.

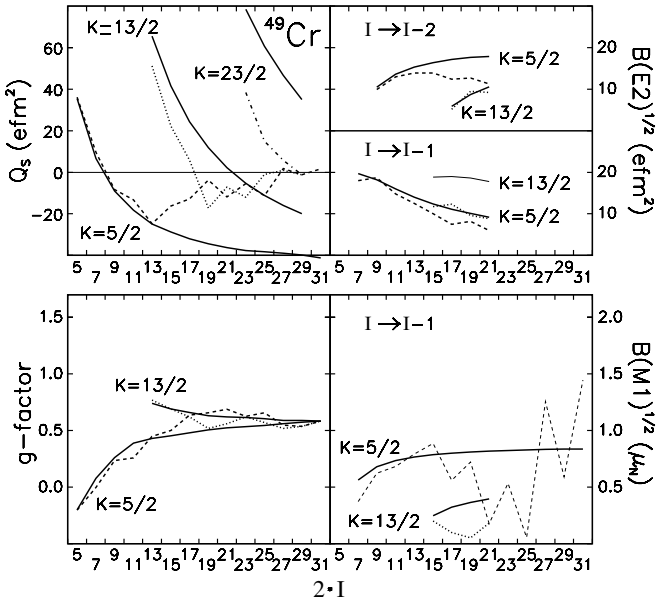

FIG. 5. Calculated em moments in ^{49}Cr. Rotor ($\beta^* = 0.28$), solid line; SM, dashed ($K = 5/2$) and dotted ($K = 13/2$) lines.

For the pure $\pi f_{7/2}^p \otimes \nu f_{7/2}^n$ configuration, the g factor can be estimated with the additivity rule:

$$g = \frac{g_p + g_n}{2} + \frac{g_p - g_n}{2} \frac{I_p(I_p+1) - I_n(I_n+1)}{I(I+1)}. \qquad (6)$$

If one assumes the effective values $g_n = -0.30$ and $g_p = 1.38$, instead of the Schmidt values of -0.547 and 1.655, respectively, one gets for the terminating states the mean reproduction of SM values reported in the last column of Table II. These empirical values will be adopted in semiclassical considerations. In the case of the mirror nucleus ^{53}Co, the isovector part, i.e., the second addendum in Eq. (6), changes sign. Looking at Table II, we see that the SM isoscalar part agrees with the empirical value of 0.54, calculated as the average of the values for a mirror pair.

The slope of the g curve at low spin follows rather closely a rotor behavior, whereas the asymptotic value at high spins is not the usual $g_R \simeq 0.5$, but the curve is adjusted to $g = 0.77$ at $I = 19/2$, according to Eq.(6), because only two proton holes and one neutron hole are active. The slope of $B(M1)$ is also consistent with a rotor behavior, apart from a staggering approaching termination, which is characteristic of a $1f_{7/2}^{-3}$ description [43].

To conclude, ^{53}Fe can be considered a paradigm of the fragility of the collective rotation in $1f_{7/2}$ nuclei and of the intrinsic change of regime along the gs band.

The nucleus ^{43}Sc becomes particlelike ($\gamma = 60^\circ$) in proximity of the termination, to which case a negative Q_s value pertains. It must be stressed, therefore, that an ambiguity arises for nuclei at the beginning of the shell, since for them a negative Q_s value is predicted both before and after the shape transition.

B. ^{49}Cr

The next nucleus to be examined is the $N = Z + 1$ ^{49}Cr, which has been studied in detail in Refs. [15,16,18]. A partial level scheme of ^{49}Cr is shown in Fig. 4, up to the termination at $31/2^-$. Only the lower members of the 1-qp sidebands are reported, and approaching the termination, only states with prevailing $1f_{7/2}^n$ configuration. Few levels were added with respect to Refs. [15,16], which were observed in a recent experimental work [18], where also a detailed comparison with PRM was made. Calculated levels are also organized in bands.

SM calculations are able to reproduce well the observed levels. The gs band is described at low spins as a $K^\pi = 5/2^-$ band based on the $\nu[312]5/2^-$ Nilsson orbital [4,16]. The 1-qp sidebands with $K = 1/2$, 7/2, and 3/2 are described with Nilsson orbitals $[321]1/2^-$, $[303]7/2^-$, and $[321]3/2^-$, respectively. Only the first two are reported in Fig. 4. A 3-qp band with $K^\pi = 13/2^-$ is also observed, which is predicted by breaking a $[321]3/2^-$ proton pair, lifting one of them into the $[312]5/2^-$, and coupling the three unpaired particles to the maximum, K value.

The measured lifetimes lead to an initial β^* value of 0.28 for the gs band, which was adopted in Fig. 5 where the SM em properties are compared with those of the rotational model. The Q_s value of the $K^\pi = 13/2^-$ bandhead is 51.2 $e\,\mathrm{fm}^2$, which corresponds to $\beta^* = 0.24$. The smaller deformation is reasonable owing to the high spin, which reduces the number of possible interacting nucleons in the $2p_{3/2}$ orbital and thus the collectivity. Moreover, some mixing is also present.

In the same figures, a 5-qp band with $K^\pi = 23/2^-$ is reported which is obtained by additionally breaking a $[321]3/2^-$ neutron pair and lifting one of them to the $[303]7/2^-$ orbital. It is merely incipient since it terminates at the common termination $31/2^-$ ($Q_s = 1.6\ e\,\mathrm{fm}^2$). The calculated Q_s moment of the $K^\pi = 23/2^-$ bandhead is 38.8 $e\,\mathrm{fm}^2$, corresponding to a $\beta^* = 0.16$ value. The yrare $25/2^-$ state is mixed so that it decays to the yrast $23/2^-$ state with a fast $M1$.

The magnetic moment of the $I^\pi = K^\pi = 13/2^-$ state is given semiclassically by the sum of the longitudinal component along the total spin. In the $1f_{7/2}^n$ space, taking $\cos\theta = K/j$, one gets $g = \mu/I \simeq 2/13[1.38(3/2 + 5/2) - 0.3(5/2)]$, so that the g factor of the $13/2^-$ level is $g = 0.74$, in agreement with the SM value of 0.77. The curves of g and $B(M1)$ adopt such empirical values. It has to be noted that in Fig. 4 some SS is observed at low spin, whose size is not reproduced by PRM and CSM [44].

Above the backbending at $19/2^-$, the SS of the gs band becomes so large that the ordering of spin values is inverted. This indicates a change of regime, which cannot be associated to a band crossing, neither experimentally nor theoretically [15]. Also, the Q_s plot of the ^{49}Cr gs band shows that collective rotation starts to be severely damaged above $I^\pi = 13/2^-$. In fact, at low spin the values follow the rotor predictions, and become rapidly negative, according to Eq. (1), but they start to rise around $13/2^-$, becoming nearly zero at the backbending level $I^\pi = 19/2^-$, presumably because of the influence of the $v = 3$ termination, as will be further discussed together with the similar backbending in ^{48}Cr.

This interpretation is confirmed by the g-factor curve, which is adjusted at $I = 31/2$ to the empirical value 0.57, obtained from the additivity rule (the SM value is 0.59). The SM g factor ranges around 0.65 at spin $19/2^-$, which is larger than the rotor value of 0.53, while it is halfway to the value of 0.79 for the termination of $v = 3$ states.

Above $I \simeq 15/2$, single-particle features start to become evident. In fact, the staggering of $B(M1)$ values approaching band termination (confirmed very well experimentally [16]) is a $1f_{7/2}^n$ phenomenon [43] that cannot be reproduced by a deformed mean-field model.

C. ^{51}Mn

Experimental levels and $B(E2)$ and $B(M1)$ values of the $N = Z + 1$ nucleus ^{51}Mn have been recently found to agree with SM calculations [20]. The gs band is interpreted with the same Nilsson configuration $[312]5/2^-$ as ^{49}Cr, while the termination now occurs at $27/2^-$. The experimental level scheme of ^{51}Mn shown in Fig. 6 includes data from NDS and the recent Ref. [45]. The $K^\pi = 5/2^-$ gs band resembles that of ^{49}Cr, apart from a larger SS, up to the backbending at $17/2^-$, pointing to a similar deformation. The calculated gs g factor is 1.359 in agreement with the experimental 1.427(1) and not far from the effective value for a $1f_{7/2}$ proton. Calculated em observables are plotted in Fig. 7. The larger SS is correlated with the staggering of $B(M1)$ and g-factor values. CD could produce staggering only at rather high spin, while the observed one starts early. Such early staggering is considered an indication of triaxiality, associated with $\gamma < 0$. The larger SS in ^{51}Mn with respect to ^{49}Cr can be interpreted as a sign of substantial triaxiality. Staggering was observed also in the CED values [46,47], which thus may be also related to triaxiality. In spite of that, the axial rotor formulas with $\beta^* = 0.26$ reproduce qualitatively the SM values for Q_s and $B(E2)$ at low spins. It has to be noted that above $15/2^-$, the $B(E2)$ values for $\Delta I = 1$ transitions become very small.

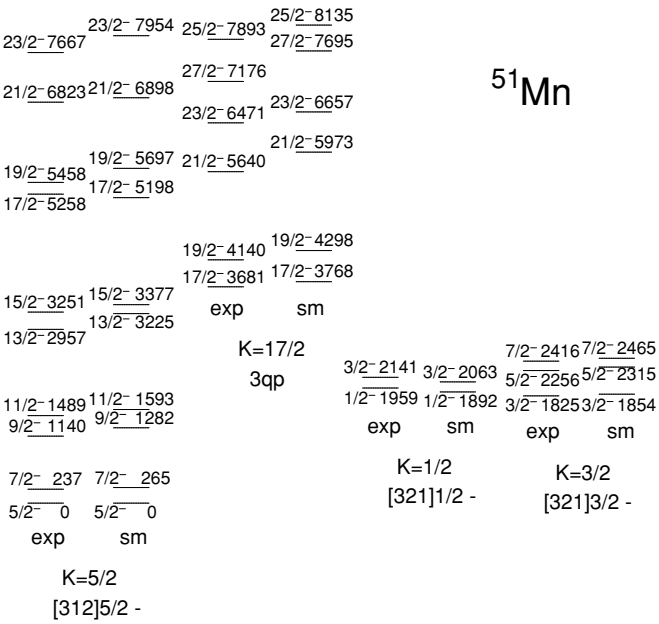

FIG. 6. Comparison of experimental negative parity levels in ^{51}Mn with SM predictions.

The 3-qp band is produced by breaking a $[312]5/2^-$ neutron pair, lifting one of them into $[303]7/2^-$, and coupling the three unpaired particles to the maximum K value. The

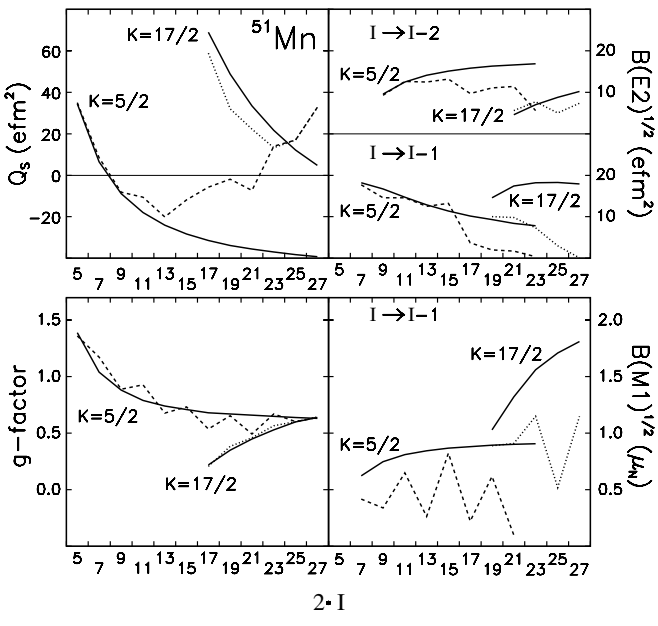

FIG. 7. Calculated em moments in ^{51}Mn. Rotor ($\beta^* = 0.26$), solid lines; SM, dashed ($K = 5/2$) and dotted ($K = 17/2$) lines.

interpretation of the yrast $17/2^-$ level as a $K^\pi = 17/2^-$ bandhead was already proposed [9,48] to explain the observed anomaly of CED values starting at $I = 17/2$. It is confirmed by the predicted large Q_s value of $56.3\,e\,\mathrm{fm}^2$, which corresponds to $\beta^* = 0.22$, according to Eq. (1). This value may be underestimated owing to some configuration mixing. Moreover, the low SM value of its g factor (0.206) is related to the fact that now the 3-qp state is formed by one $K = 5/2$ proton and two neutrons with $K = 5/2$ and 7/2, respectively. Semiclassically, as previously made in ^{49}Cr, $g = \mu/I \simeq 2/17[1.38 \cdot 5/2 - 0.30(3/2 + 5/2)]$, resulting in a g factor of 0.26 for the $17/2^-$ level.

The calculated yrast level $19/2^-$ is assigned to the $K = 17/2$ band in virtue of its em properties. The $B(E2)$ value of the transition to the yrast $17/2^-$ level is large, as expected for an intraband transition, while the one to the yrast $15/2^-$ is small. Its g factor is 0.39, much smaller than the rotor value of 0.60, obtained adjusting the rotor curve to the empirical value of 0.63 at $27/2^-$ (the SM value is 0.64).

The yrare $17/2^-$ level belongs to the gs band since its $E2$ decay to the yrast $13/2^-$ is favored. The yrare $19/2^-$ state was not observed. It is predicted to have $g = 0.67$, higher than the rotor value of 0.58 and halfway to the $v = 3$ value of 0.79. Its Q_s value is slightly positive.

The level spacing of the gs band changes above the $13/2^-$ level, pointing to a change of regime as in ^{49}Cr; but, while in the case of ^{51}Mn the SS decreases, in ^{49}Cr it increases. The reason for the different behavior is not understood. The change of regime is signaled also by the change of Q_s and $B(E2, I \to I-1)$ values above $17/2^-$.

The positive value of Q_s at the terminating level $27/2^-$ ($32.7\,e\,\mathrm{fm}^2$) is due to the noncollective prolate shape of the $\pi^{-3}\nu^{-2}$ configuration. The corresponding β^* is 0.09. The two bands with $K = 5/2$ and 17/2 loose collectivity with increasing spin, and their Q_s values become positive.

As for ^{53}Fe, the observed positive Q_s value at $23/2^-$ and above is incompatible with rotational alignment, since the Q_s value would be expected to be negative in that case.

Yrast high-K bands of natural parity can occur only in the second half of the $1f_{7/2}$ shell because one needs to deal with the high-K Nilsson orbital. In fact, the reason why the $K^\pi = 17/2^-$ crosses the gs band while the $K^\pi = 13/2^-$ band in ^{49}Cr does not is that their excitation energies are similar, but the spin values are higher in the former case.

Applying the Nilsson diagram to look for a possible 5-qp band as in ^{49}Cr, one gets $K^\pi = 27/2^-$; but $I^\pi = 27/2^-$ is the terminating state, so a 5-qp band does not exist in ^{51}Mn.

D. ^{51}Cr

The $N = Z + 3$ nucleus ^{51}Cr has been recently discussed [20], but the band crossing of the gs band was not recognized. The gs band is based in this case on the Nilsson orbital $\nu[303]7/2^-$. The experimental levels, taken from NDS, are displayed in Fig. 8 where they are compared with SM calculations up to the termination at $23/2^-$ ($Q_s = 6.9\,e\,\mathrm{fm}^2$). Since its configuration is $\pi^{-4}\nu^{-1}$, the positive value is due to the neutron-hole configuration. The calculated levels reported

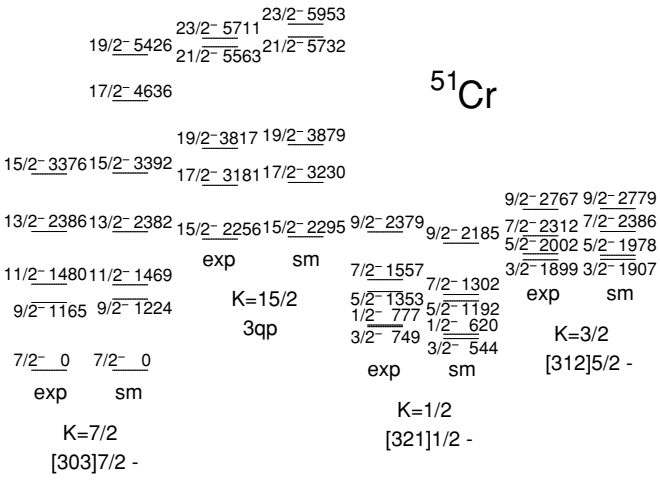

FIG. 8. Comparison of experimental negative parity levels in ^{51}Cr with SM predictions ($s = 3$).

here were obtained with an $s = 3$ truncation. Calculations were made also in full pf configuration space, but a worse average agreement by about $\simeq$50 keV was obtained, possibly pointing to a somewhat too large contribution of the $1f_{5/2}$ orbital. Relevant SS occurs at the yrast $9/2^-$ level, but it decreases above that, in contrast with ^{49}Cr. The deformation parameter at low spins is $\beta^* = 0.21$, much smaller than in ^{48}Cr.

The yrast $15/2^-$ level is interpreted as the head of the 3-qp band obtained by lifting one proton from the $[321]3/2^-$ orbital to the $[312]5/2^-$ one and coupling the three unpaired nucleons to the maximum value of K. The empirical g factor is $g = \mu/I \simeq 2/15[1.38(3/2 + 5/2) - 0.30(7/2)] = 0.60$, while the SM value is 0.69.

The em observables are plotted in Fig. 9, and they resemble qualitatively those of ^{49}Cr.

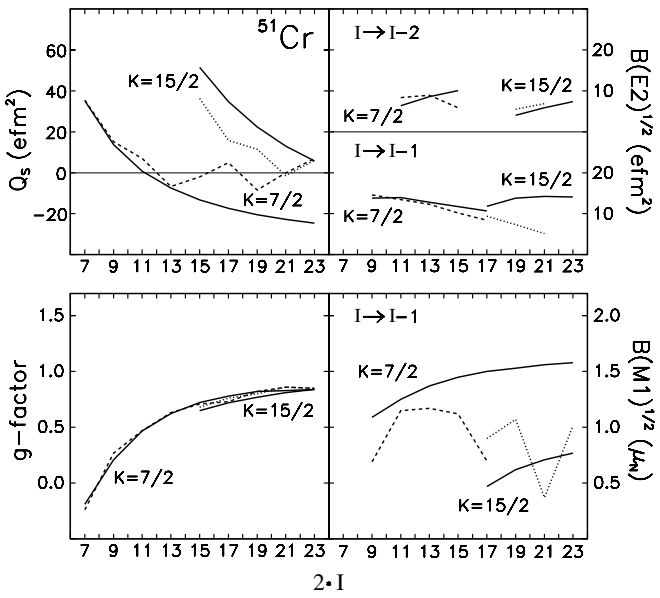

FIG. 9. Calculated em moments in ^{51}Cr. Rotor ($\beta^* = 0.21$), solid lines; SM, dashed ($K = 7/2$) and dotted ($K = 15/2$) lines.

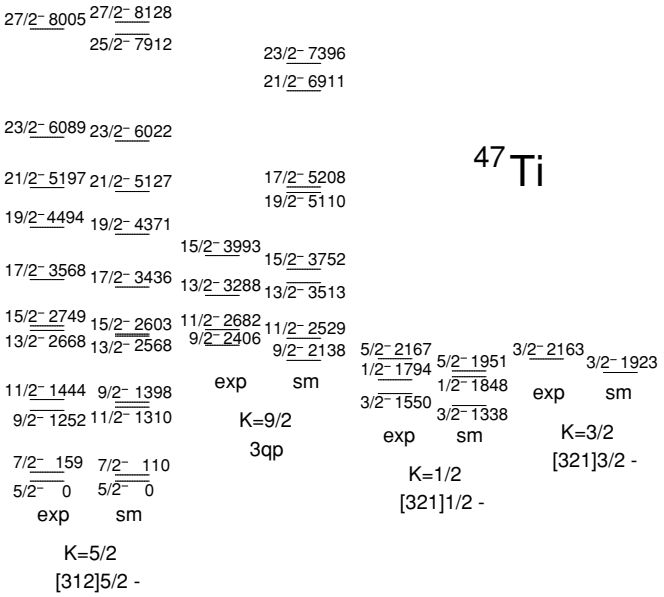

FIG. 10. Comparison of experimental negative parity levels in ^{47}Ti with SM predictions.

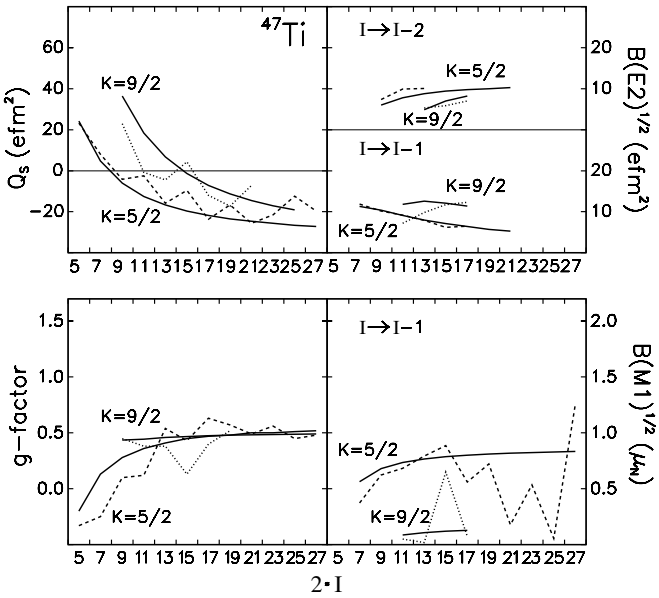

FIG. 11. Calculated em moments in ^{47}Ti. Rotor ($\beta^* = 0.22$), solid lines; SM, dashed ($K = 5/2$) and dotted ($K = 9/2$) lines.

The g-factor values of both bands converge at $I = 23/2$ to the empirical value 0.87 (the SM value is 0.85). The agreement of SM values with the rotor prediction is remarkable.

E. ^{47}Ti

In the $N = Z + 3$ nucleus ^{47}Ti, the gs band is based on the $\nu[312]5/2^-$ orbital as in ^{49}Cr and shows relevant SS as in ^{51}Mn. Levels were taken from NDS. As shown in Fig. 10, no band crossing occurs along the gs band, since the $K = 9/2$, 3-qp band, resulting from the lifting of one proton from the $[321]1/2^-$ orbital to the $[312]3/2^-$ one, is largely non-yrast. The semiclassical g factor of the sideband head is $g = \mu/I \simeq 2/9[1.38(1/2 + 3/2) - 0.30(5/2)] = 0.45$ while the SM value is 0.44. The terminating Q_s value is –19.6 e fm^2, showing that the shape associated with the π^2 configurations largely prevails over that of the ν^{-3} one. This occurs also in a restricted $f_{7/2}^n$ space. The empirical g-factor value at termination is 0.45, in agreement with the SM value 0.48.

^{47}Ti has been discussed in detail in Ref. [4] as a distinct case of incipient rotational collectivity, since the Q_s values follow the expectation for a rotating prolate nucleus nearly up to the termination at $I = 27/2$. This is illusory, however, since approaching termination the negative value of Q_s is associated with an oblate noncollective shape and not a prolate collective one. The values of Q_s displayed in Fig. 11 do not reveal the change of regime, which is, however, signaled by the decrease of SS above $15/2^-$, as in ^{51}Mn and ^{51}Cr. The nucleus is not much deformed, so the configurations are quite mixed. The particularly large perturbation of the sideband at 15/2 can be interpreted as being due to the mixing with a 3-ν configuration. In this case, a $K = 15/2^-$ band results from the parallel coupling of neutron orbitals [321]3/2, [312]5/2, and $[303]7/2^-$, which produces both the positive value of Q_s and the small value of g. Similarly, the inversion of sideband levels $19/2^-$ and $17/2^-$ may be caused by the interaction with a $19/2^-$ 5-qp band, which is obtained by further breaking a neutron pair. The SS at low spins presents a problem since PRM and CSM with $\gamma \leqslant 0$ cannot explain its entire size. This may point to some limits of the mean-field approximation.

F. ^{47}V and ^{49}V

Large SS at low spin is observed in the odd V isotopes ^{45}V, ^{47}V, and ^{49}V. Their level schemes are basically similar at low excitation energies, as they are all based on the $[312]3/2^-$ Nilsson orbital, giving rise to a $K^\pi = 3/2^-$ band. The three isotopes are characterized by having very close yrast 3/2, 5/2, and 7/2 levels, even if the ordering changes. This can be explained by a sensible CD, induced by the mixing with the orbital $[330]1/2^-$ caused by pairing, which is reasonably well reproduced by PRM calculations. Termination occurs at $27/2^-$ in ^{45}V and ^{49}V, while at $31/2^-$ in ^{47}V. The 3-qp band is expected to have $K = 7/2$, 11/2, and 15/2 in ^{45}V, ^{47}V, and ^{49}V, respectively.

The level scheme of the $N = Z + 1$ nucleus ^{47}V is shown in Fig. 12. The gs band has been discussed in Ref. [16], where the experimental $B(E2)$ and $B(M1)$ values along the gs band turned out to agree reasonably well with theory. Its deformation at low spins is nearly as large as that of ^{49}Cr, but band mixing is larger than in ^{49}Cr. The calculated $17/2^-$ level belonging to the gs band is the yrare one, while the yrast $17/2^-$ level belongs essentially to the predicted $K = 11/2$ 3-qp band [48]. Unfortunately, both $17/2^-$ levels were not observed experimentally. The empirical g factor of the $K = 11/2^-$ bandhead is $g = \mu/I \simeq 2/11[1.38(3/2) - 0.30(3/2 + 5/2)] = 0.16$ to be compared with the SM value 0.18. According to Fig.12, the yrast levels $21/2^-$ and $25/2^-$ also belong essentially to the sideband, even if they are mixed. As shown in Fig. 13, staggering is observed at low spin for

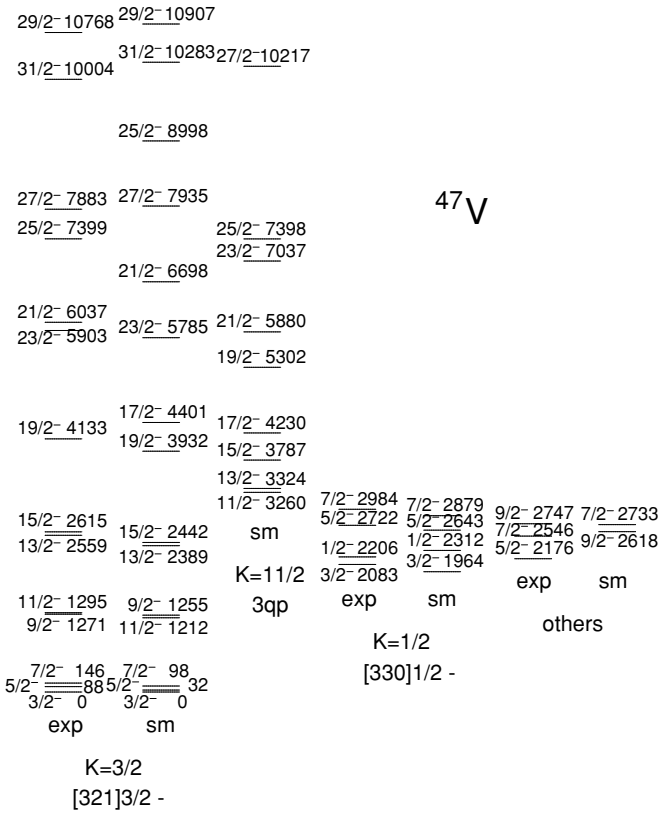

FIG. 12. Comparison of experimental negative parity levels in ^{47}V with SM predictions.

both Q_s and g. This may be associated with triaxiality, but it is not easy to disentangle the effects of CD.

The Q_s values become smaller above $I^\pi = 17/2^-$ and remain constant up to the termination at $31/2^-$ ($Q_s = -14.4\,e\,\mathrm{fm}^2$). The empirical g-factor value at the termination is 0.51, in agreement with the the SM value 0.53. The SS increases with spin leading to ordering inversion. According to Ref. [4], the g-factor values around $19/2^-$ reflect a $v = 3$ termination, but contrarily to ^{49}Cr, no backbending is observed at the change of regime. In this nucleus, it is particularly difficult to assign side levels to 1-qp bands, since there is no regularity. The $K = 1/2$ band is denoted by $[330]1/2^-$. The experimental 5/2 level at 2176 does not have a calculated counterpart.

Figure 14 shows that the level scheme of the $N = Z + 3$ nucleus ^{49}V is well predicted by SM calculations and it presents analogies with that of ^{47}V. At the termination, the Q_s value is –8.5 $e\,\mathrm{fm}^2$, showing that the proton-hole shape prevails. It has the largest SS among the three isotopes, and its gs band is expected to be crossed by a $K^\pi = 15/2^-$ 3-qp band, which is observed experimentally. Its bandhead is the yrare $15/2^-$ with $Q_s = 33.0\,e\,\mathrm{fm}^2$, while the member with $I = 17/2$ is yrast. The larger SS is probably related with triaxiality, reflecting a high configuration mixing among Nilsson configurations. For this reason, a limited number of levels is reported in Fig. 15, so only PRM predictions are displayed for sidebands. The g factor of the $K = 15/2$ bandhead is predicted to be $g = \mu/I \simeq 2/15[1.38(3/2) - 0.30(5/2 + 7/2)] = 0.04$,

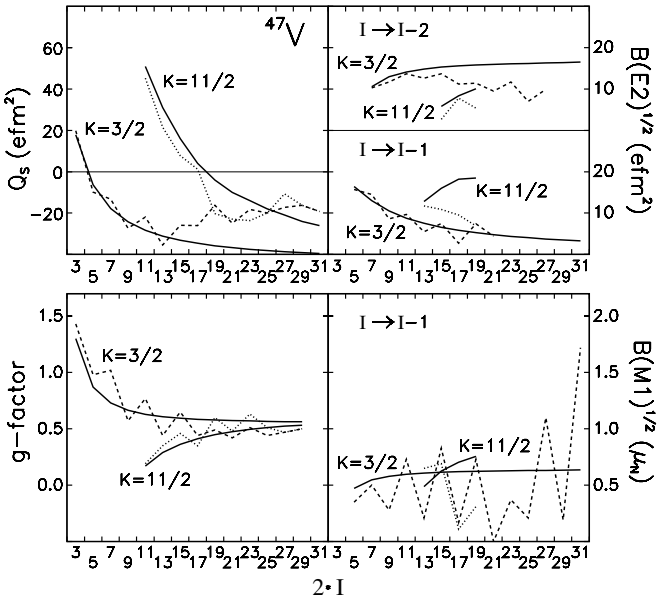

FIG. 13. Calculated em moments in ^{47}V. Rotor ($\beta^* = 0.26$), solid lines; SM, dashed ($K = 3/2$) and dotted ($K = 11/2$) lines.

which greatly differs from the SM value of 0.34, indicating mixing effects, which apparently also lower its Q_s value in Fig. 15.

The empirical g-factor value at the termination is 0.63, in agreement with the the SM value 0.66.

The level schemes of ^{45}V and of its mirror ^{45}Ti are identical, apart for Coulomb effects. Their level schemes are somewhat perturbed at low spin by intruder two- and four-hole configurations. They will not be further discussed here because their level schemes are not sufficiently well known to bring relevant new information.

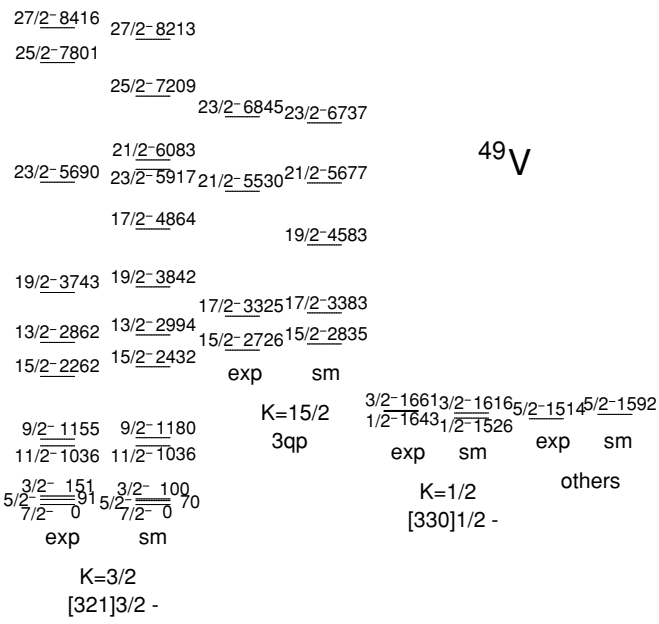

FIG. 14. Comparison of experimental negative parity levels in ^{49}V with SM predictions.

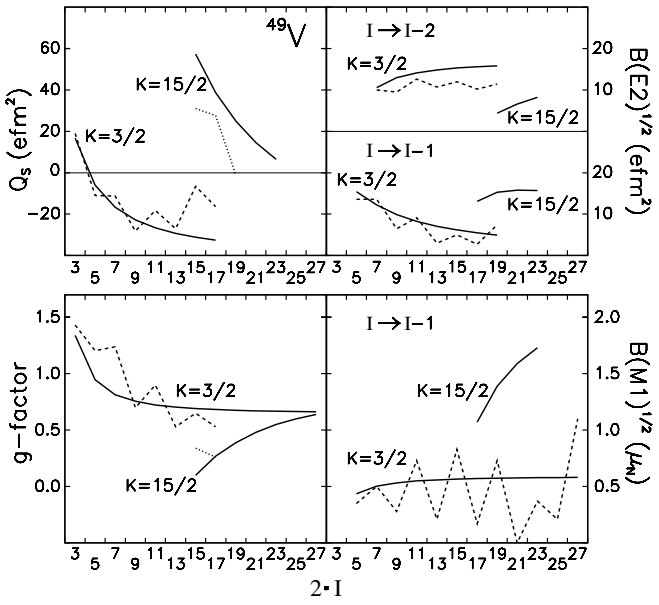

FIG. 15. Calculated em moments in ^{49}V. Rotor ($\beta^* = 0.25$), solid lines; SM, dashed ($K = 3/2$) and dotted ($K = 15/2$) lines.

G. ^{48}Cr

In the last 10 years, ^{48}Cr has been addressed by several theoretical studies as its understanding is considered to be of strategic importance. The gs band shows a backbending, whose interpretation is still somewhat controversial 10 years after its observation [49] and which will be again discussed in the next subsection. An updated experimental level scheme is reported in Fig. 8. Yrast levels were taken from Ref. [7], while yrare levels are essentially from a recent work [50], where spin-parity assignments were not precisely determined. It is assumed that all experimental side levels in Fig. 16 have positive parity, on the basis of the following argument: in ^{48}Cr a negative parity band with $K^\pi = 4^-$, whose bandhead is at 3532 keV, was determined in Ref. [7], where it was described as the coupling of the [202]3/2$^+$ orbital with the [312]5/2$^-$ one. This band is well reproduced by SM calculations, which predict that the $K^\pi = 1^-$ band originating from the antiparallel coupling lies at an energy more than 1 MeV higher. The reliability of these predictions is stressed by the fact that the lowest terms of both bands are correctly reproduced in ^{50}Cr [48].

The observed lowest side levels [50] are tentatively assigned to the calculated bands according to their energy and decay scheme. The very good agreement is likely to be not fortuitous. The original SM calculations using KB3 [2] differ from the present ones by at most hundred keV for any reported level and predict very similar em moments within few percents. In the rest of the subsection, we will refer principally to calculated level energies. The structure of the ^{48}Cr gs band was extensively discussed in the frame of SM [2]. As shown in Fig. 16, the gs band develops without band crossing up to the termination at 16^+. This was also confirmed by CHFB calculations [2,11]. In Fig. 17, a deformation parameter

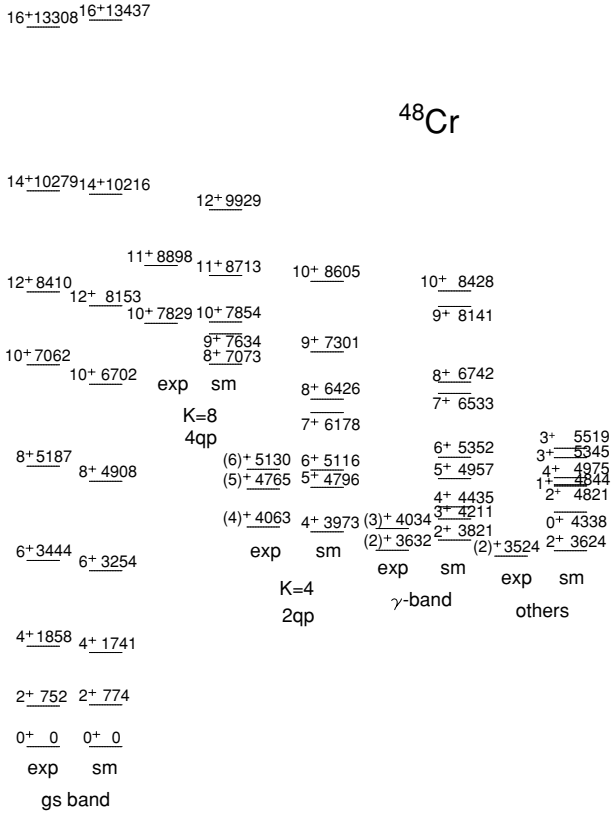

FIG. 16. Comparison of experimental positive parity levels in ^{48}Cr with SM predictions.

$\beta^* = 0.31$ is assumed for the initial deformation. The lowest 2-qp band is formed with $K^\pi = 4^+$ by promoting one neutron or one proton from the [321]3/2$^-$ to the [312]5/2$^-$ orbital [8]. Its head is the yrare 4^+ which lies 2.3 MeV above the yrast 4^+. It is rather unexpected that its Q_s value is less than half

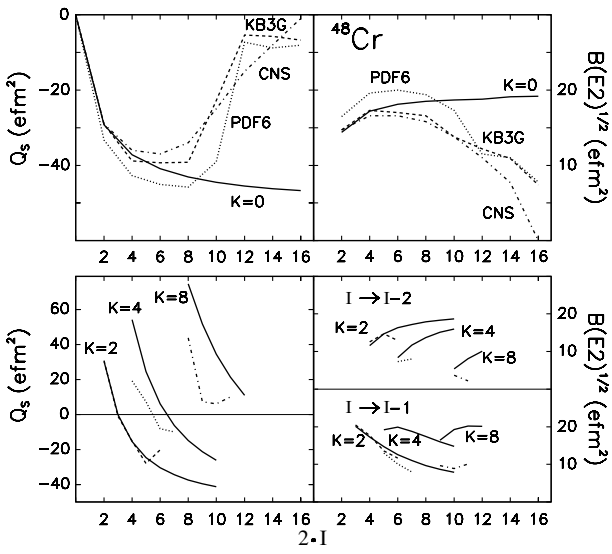

FIG. 17. Upper panels: Comparison of rotor ($\beta^* = 0.31$) estimates with some SM predictions for the gs band in ^{48}Cr. Lower panels: Calculated em moments in ^{48}Cr. Rotor, solid lines; SM, dashed ($K = 2$), dotted ($K = 4$), and dot-dashed ($K = 8$) lines.

the rotor prediction (Fig. 17, lower panels); nevertheless, the band develops rather regularly up to 8^+. The predicted band shows SS and the $B(E2)$ value of transition connecting its head to the fourth 4^+ level at 4975, built also mainly on a $1f_{7/2}^n$ configuration, is 163.0 $e\,\mathrm{fm}^2$. These features suggest triaxiality, which could explain the low Q_s value of the yrare 4^+ level. The antiparallel coupling would give rise to a 2-qp $K^\pi = 1^+$ band. The lowest 1^+ level is predicted at 4844 keV. The corresponding experimental level is not known, but the prediction has to be considered reliable since in ^{50}Cr the yrast 1^+ is at 3629 keV, while theory gives the precise estimate of 3539 keV. A favored connection of the yrast 1^+ level with the fourth 2^+ level at 4821 keV ($B(E2) = 280.6\ e\,\mathrm{fm}^2$) is the only indication of an incipient $K^\pi = 1^+$ band, which gets exhausted with the third 3^+ level at 5519 keV ($B(E2) = 86.1\ e\,\mathrm{fm}^2$).

The yrare 2^+ level at 3624 keV has $Q_s = 20.7\ e\,\mathrm{fm}^2$ and is connected with a $B(E2)$ rate of 104.0 $e\,\mathrm{fm}^2$ to the yrare 3^+ level at 5345 keV. These features are consistent with being a $K = 2$ bandhead with a reduced deformation. It may be also triaxial, but its interpretation is uncertain.

All levels without clear collective properties are grouped on the rightmost side of Fig. 16.

As shown in the same figure, a 4-qp band with $K^\pi = 8^+$ is predicted to start at an excitation energy of 7073 keV, about twice as large as that for the $K^\pi = 4^+$ bandhead, being due to the simultaneous breaking of a proton and a neutron pair. Its Q_s value is 43.8 $e\,\mathrm{fm}^2$, corresponding to $\beta^* = 0.18$. The observed yrare 10^+ level decays mainly to the yrast 8^+ level with a 2644 keV transition and has a weak branch of 768 keV to the yrast 10^+ one [51]. This is expected by SM calculations for the member of the $K^\pi = 8^+$ band. The yrare 12^+ is predicted to lie 2 MeV above the yrast one and to belong essentially to the $K^\pi = 8^+$ band. At a similar excitation energy of the $K^\pi = 8^+$ band, a 4-qp $K^\pi = 2^+$ band could also be expected, of which, however, no evidence exists.

A $K^\pi = 2^+$ band is predicted to start at 3821 keV and to be well deformed (Fig. 17, lower panels). The peculiar nature of this band is revealed by its very fragmented wave function, where the $1f_{7/2}^n$ configuration contributes less than 1% to the wave function of the lowest members, while it has a contribution of about 20% for the 2^+ level of the gs band and about 40% for the $K^\pi = 4^+$ bandhead. That band is therefore a good candidate for being the γ band. Relevant mixing with the $K = 4$ band, as well as a large SS, occurs above 6^+.

H. ^{48}Cr gs band backbending

The backbending of the ^{48}Cr gs band was well reproduced 10 years ago by SM calculations in the full *pf* space [1]. It is accompanied by a peculiar behavior of the Q_s values (Fig. 17); the values are consistent with an axially prolate description up to $I^\pi = 8^+$, but above that, they rapidly become nearly zero, indicating a spherical shape. If one repeats the calculations with any other of the mentioned effective interactions the behavior is essentially the same. CHFB [2,11] and CNS [12] calculations estimate $\gamma \simeq -15^\circ$ at the backbending region. In Fig. 17, the CNS predictions are displayed for comparison, while the CHFB ones would be similar. The axial description is good up to 6^+. The predicted triaxiality somewhat improves the quality of Q_s values. In fact, Q_s is related to $Q_\circ$ by Eq. (1), which for $K = 0$ becomes $Q_s = -Q_\circ I/(2I + 3)$, where

$$Q_\circ = \frac{6}{\sqrt{5\pi}} ZeR_0^2\beta \sin(30 + \gamma). \tag{7}$$

$Q_\circ$ is thus smaller than in the case of axial symmetry, while $B(E2)$ values increase according to the relation

$$Q_t = 2\sqrt{\frac{3}{5\pi}} ZeR_0^2\beta \cos(30 + \gamma). \tag{8}$$

One should comment, however, that both CNS [12] and standard CHFB calculations [2] cannot reproduce well the backbending and the drastic reduction of Q_s above $I^\pi = 10^+$. These anomalies may lead one to guess a band crossing with the slightly deformed 4-qp $K^\pi = 2^+$ band, as claimed in a PSM analysis [13]. However, as previously discussed, the presence of that band has to excluded. Since the yrare 12^+ level lies about 2 MeV higher than the yrast level, one has to conclude that what occurs is an intrinsic change of structure, that is not well described within a mean-field approximation. One is led to relate these facts to the pairing interaction, an important ingredient of any realistic interactions, which is not accounted for by the mentioned deformed mean-field theories. This hypothesis was first supported by SM calculations, while keeping the information on the seniority of the states [14]. This was confirmed in Ref. [31], where, using the realistic interaction KLS, backbending predicted researchers at $I = 12$ in the $\pi(fp)^4\nu(fp)^4$ configuration space (^{48}Cr), at $I = 16$ in the $\pi(gds)^4\nu(gds)^4$ space and at $I = 14$ in the $\pi(fp)^4\nu(gds)^4$ space. The backbending spin values are just the terminations in the $\pi 1f_{7/2}^2\nu 1f_{7/2}^2$, $\pi 1g_{9/2}^2\nu 1g_{9/2}^2$, and $\pi 1f_{7/2}^2\nu 1g_{9/2}^2$ configuration spaces, giving a clear indication that the backbendings are related to terminations in $v = 4$ subspaces. The same reference showed also that an interaction with only monopole and quadrupole terms cannot reproduce the backbendings. Since it has been shown that the schematic interaction $P + QQ$, containing only monopole, pairing, and quadrupole terms, simulates closely realistic interactions for the mentioned aspects [27], one is led to conclude that pairing is related to both the backbending and the Q_s-plot anomaly. Moreover, Ref. [52] showed that by that subtracting the pairing contribution to the realistic interaction KB3, the backbending essentially disappears in ^{48}Cr.

The proposed explanation is the following: the configuration mixing decreases with increasing spin, together with the deformation. The percentages of the $(1f_{7/2})^8$ configuration are 33, 37, 51, 66, 72, and 88 for levels of spin 6, 8, 10, 12, 14, and 16, respectively. When the deformation becomes low enough, the discussed effects related to pairing become apparent. The mentioned deformed mean-field theories cannot predict these effects, but they describe correctly the structure at the band termination.

The backbending at $19/2^-$ in ^{49}Cr is apparently due to a similar mechanism applied to $v = 3$. A similar effect also occurs in $1g_{9/2}^n$ nuclei. The gs band of ^{93}Pd, with a configuration $\pi^{-4}\nu^{-3}$, has a backbending at $25/2^+$ [53], which

is the highest spin in a $\pi^2\nu$ subspace. The level scheme is well reproduced by SM calculations. By projecting the $25/2^+$ state wave function into states with definite seniority, a $v=3$ percentage of about 50% was found. The band appears to be slightly collective already at rather low spins, indicating that approaching the $N=Z=50$ double shell closure the polarizing action of the $2d_{5/2}$ orbital on the $1g_{9/2}$ one is less effective than that of the $2p_{3/2}$ orbital on the $1f_{7/2}$ one, because of the larger energy gap between the orbitals.

I. ^{52}Fe and ^{44}Ti

The experimental level scheme of ^{52}Fe is taken from NDS and Ref. [42]. The fact that the terminating state 12^+ lies 424 keV below the 10^+ level has an explanation similar to that for ^{53}Fe. As shown in Fig. 18, the gs band in ^{52}Fe develops rather regularly up to spin 10^+, with a smaller moment of inertia than observed for ^{48}Cr. The calculated scheme was obtained with truncation $s=3$. Clear correspondence is evident between experiment and theory, despite the somewhat worse agreement than obtained for ^{48}Cr.

The presence of two low-lying yrare levels 6^+ and 8^+ was already assigned to the 2-qp K = 6 band, formed by the excitation of one neutron or one proton from the $[312]5/2^-$ to the $[303]7/2^-$ orbital, but the observed interband connections point out that they are strongly mixed with the gs band [42].

The experimental yrare 2^+ and 4^+ levels, on the other hand, have to be attributed to the $K^\pi=2^+$ γ band, which lies about 1 MeV lower than in ^{48}Cr, in spite of the lower deformation. As in ^{48}Cr, the wave function of the γ band is very fragmented, while in the $K^\pi=0^+$ and $K^\pi=6^+$ bands

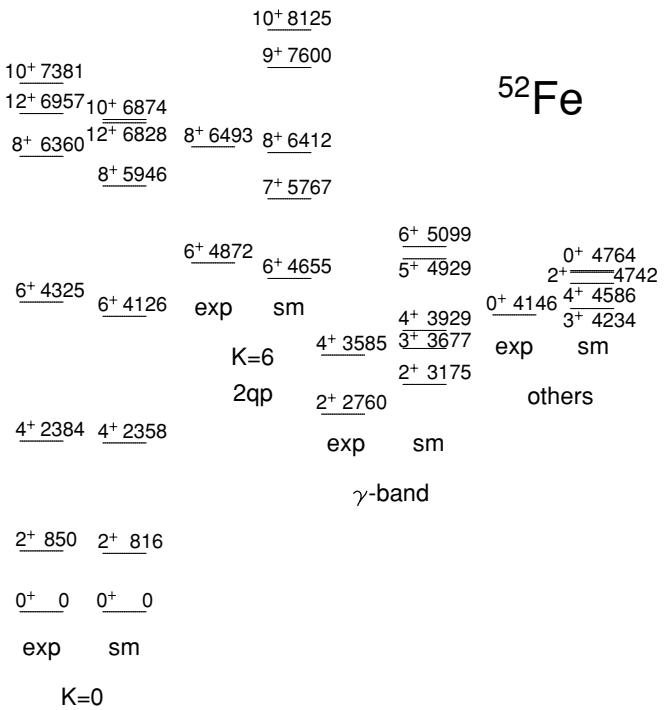

FIG. 18. Comparison of experimental positive parity levels in ^{52}Fe with SM predictions ($s=3$).

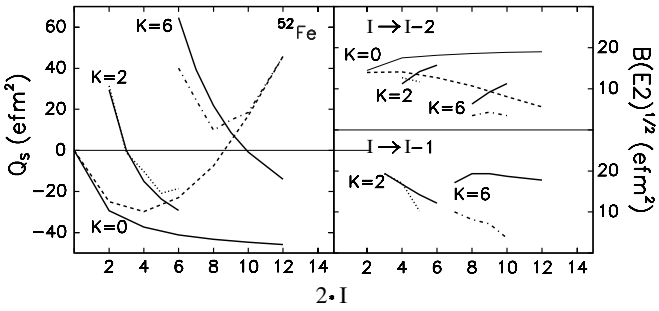

FIG. 19. Calculated em moments in ^{52}Fe. Rotor ($\beta^*=0.26$), solid lines; SM, dashed ($K=0$), dotted ($K=2$), and dot-dashed ($K=6$) lines. See text for details.

the $(f_{7/2})^{-4}$ configuration is dominant. The offset for the γ band with respect to calculations can be attributed, at least partially, to the space truncation. The γ band corresponds to a deformation $\beta^*=0.26$, as shown in Fig. 19, and develops regularly up to $I=6$. There is, however, a mixing of about 15% with the gs band, as the yrare 4^+ level is predicted to be connected to the yrast 2^+ one by a $B(E2)$ rate of 40 e fm^2. For this reason, one expects that the 4^+ level decays mainly to the yrast 2^+ level with a 2735 keV transition, while only by about 1% decays to the yrare 2^+ with a 825 keV transition.

The Q_s value of the 12^+ terminating state is calculated in the full *pf* space without any truncation to be 47.1 e fm^2, which corresponds to a deformation $\beta^*=0.12$ of the expected prolate noncollective shape. Using interactions GXPF1 and FPD6, one gets $Q_s=$ 51.2 and 58.7 e fm^2, respectively. As already noted, the gs band 6^+ and 8^+ levels are strongly mixed with the corresponding members of the $K^\pi=6^+$ band. Calculations predict an additional mixing with the γ band. Since such multiband mixing makes the interpretation difficult, the Q_s data of the $K=0$ and $K=6$ bands presented in Fig. 19 were obtained in the $1f_{7/2}2p_{3/2}$ subspace ($s=0$), where the bands do not interfere much and the plots become similar to those in ^{51}Mn. The value of the terminating Q_s is slightly reduced to 46.8 e fm^2, while the β^* parameter for the yrast 2^+ level decreases from about $\beta^*=0.26$ to 0.23.

When trying, again in the full *pf* configuration space, to get a more detailed comparison for levels approaching termination, none of the mentioned interactions can be considered fully satisfactory. The better interaction for the description of the decay of the yrast 10^+ level is GXPF1, which correctly predicts similar $B(E2)$ values toward the two lower 8^+ levels and a correct energy spacing between them. KB3G also predicts a correct spacing but with a prevailing decay to the yrast 8^+ level, while FPD6 predicts a separation of 708 keV against the experimental of 133 keV and a prevailing decay to the yrare 8^+ level. On the other hand, GXPF1 does not predict the energy inversion between the yrast 10^+ and 12^+ levels, which is well done by FPD6 and not so well by KB3G.

It seems very difficult to get reliable wave functions for spin values above 4, because of the mentioned multiband mixing. In general some offset is present in the calculations for the bandhead energies, so that a wrong mixing is calculated for near levels. It is beyond the scope of this work, even if interesting, to search for a better effective interaction.

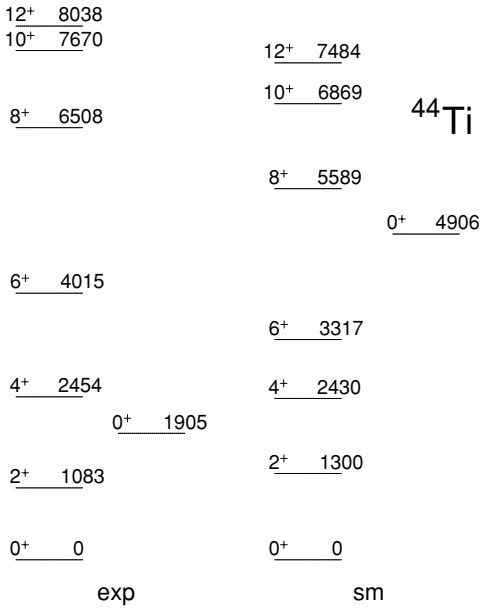

FIG. 20. Comparison of experimental gs band and yrare 0^+ levels in ^{44}Ti with SM predictions.

Using the Nilsson diagram for predicting a 4-qp band with the simultaneous excitation of both proton and neutron pairs, one gets $K = 12^+$, which, however, is the terminating state so there is no 4-qp band.

In Fig. 20, the experimental levels of the gs band of the cross-conjugate nucleus ^{44}Ti are compared with SM values. The agreement is poor. If one lifts up the SM spectrum by nearly 1 MeV in order to get the two 8^+ levels at the same height, the 0^+, 2^+, and 4^+ levels appear to be more bounded than predicted by about 1 MeV. This is attributed to the strong influence of two- and four-hole configurations, as discussed in Ref. [54]. This interpretation is confirmed by the fact that the yrare 0^+ is observed at 1905 keV, while it is predicted at 4906 keV, and it is a core-excited state, originating from two- and four-hole excitations, on which a rotational band is built. SM calculations in the two major shells do not yet provide quantitative agreement with the experimental level scheme. In this view, the 6^+ levels should be relatively unaffected. Above $I = 6$, which is the $v = 2$ termination, the level spacing increases, which may be related to the onset of the change of regime.

It is worthwhile to consider what would happen in absence of such core-core-excited contributions. The Q_s behavior of ^{52}Fe is compared with that of the cross-conjugate nucleus ^{44}Ti in Fig. 21. As in Fig. 19, calculations for ^{52}Fe were made in the $1f_{7/2}2p_{3/2}$ subspace. The adopted deformation parameter of ^{52}Fe is $\beta^* = 0.23$ in order to get a closer behavior for the lower spins. The Q_s values do not mark the change of regime in ^{44}Ti, since they are negative.

J. ^{50}Cr and ^{46}Ti

The $N = Z + 2$ nucleus ^{50}Cr has been recently studied in detail [9]. The level scheme of Fig. 22 is essentially taken

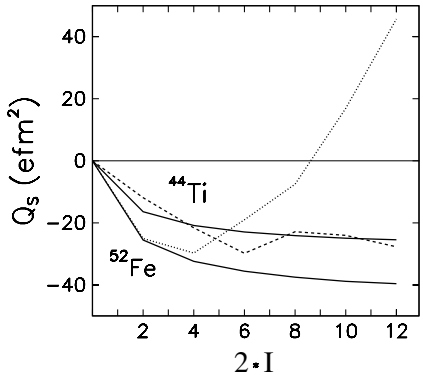

FIG. 21. Comparison of theoretical predictions for gs band Q_s values in ^{52}Fe and ^{44}Ti. Rotor values (solid lines) with $\beta^* = 0.23$ for ^{52}Fe and $\beta^* = 0.21$ for ^{44}Ti are compared with SM values (dotted and dashed lines, respectively).

from that reference, even though more calculated levels are now reported. The gs Q_s values are negative at low spin, being related to a collective prolate shape, while they become positive at the terminating level 14^+ (7.1 $e\,\mathrm{fm}^2$) as expected for an aligned-hole configuration. Bands with $K^\pi = 4^+$ and $K^\pi = 6^+$ were observed, as expected by exciting one proton and one neutron from the [321]3/2 and [312]5/2, respectively. A $K = 10$ band was also observed, which was obtained by breaking simultaneously both the neutron and the proton pairs. The em properties are displayed in Fig. 23. The smaller Q_s value of the 6^+ level is presumably due to the mixing

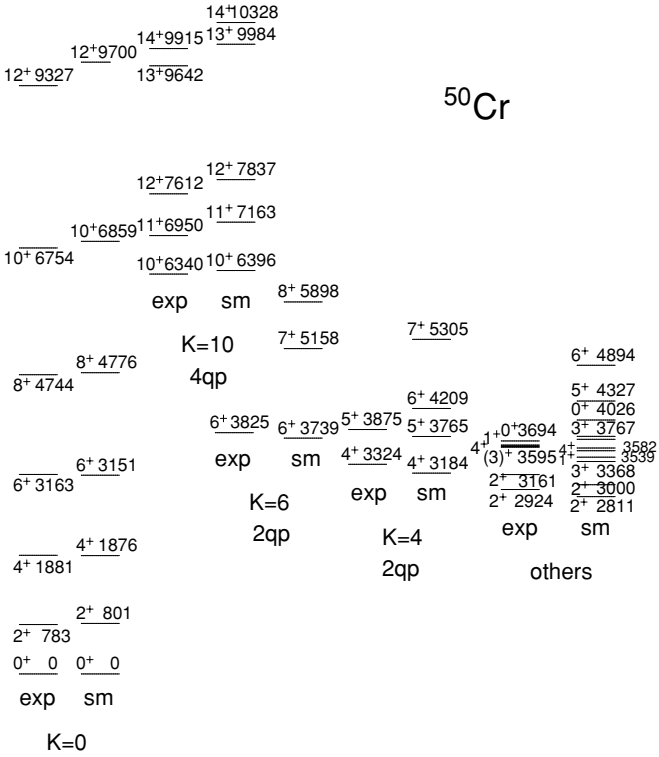

FIG. 22. Comparison of experimental positive parity in ^{50}Cr with SM predictions.

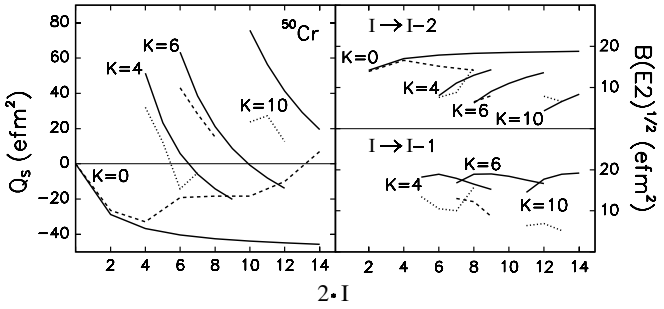

FIG. 23. Calculated em moments in ^{50}Cr. Rotor ($\beta^* = 0.28$), solid lines; SM, dashed ($K = 0$ and 6) and dotted ($K = 4$ and 10) lines.

with the head of the $K = 6$ band. This may explain the large $B(M1)$ rate between the two levels [9]. The yrast 10^+ level is experimentally identified as the head of a $K = 10$ band. SM calculations with the KB3G interaction predict a nearly 50% mixing with the 10^+ level of the gs band, which has been commented to be an overestimate [9].

Levels not belonging to previous bands are reported on the right side of Fig. 22. The level density is high both experimentally and theoretically; nevertheless, the correspondence is good, particularly for the two lower 2^+ levels.

In Ref. [9] the yrare 2^+ level observed at 2924 keV was suggested to be a member of the $K = 1$ band, following the antiparallel coupling of two unpaired nucleons. This is qualitatively confirmed by the present SM calculations since the level (calculated at 2811 keV) has $Q_s = 10.1\ e\,\mathrm{fm}^2$ and it is connected to the yrast 1^+ at 3629 keV (calculated at 3539 keV) and to the third 3^+ level calculated at 3767 keV with $B(E2)$ rates of 241 and 157 $e\,\mathrm{fm}^2$, respectively. The yrast 1^+ level is estimated to have a $B(M1)$ value of 0.35 μ_N^2 toward the gs. The experimental yrast 1^+ level has been observed in inelastic electron excitation (e, e') with a $B(M1)^\uparrow$ value of 1.10(6) μ_N^2 reported in Ref. [55], which agrees with the predicted value of 1.05 μ_N^2, using bare nucleon g factors.

The positive Q_s value 29.5 $e\,\mathrm{fm}^2$ predicted for the third 2^+ level at 3161 keV (calculated at 3000 keV) makes it a candidate for the γ bandhead. This is confirmed by the very fragmented wave function; but two 3^+ levels are predicted at 3368 and 3437 keV, which strongly mix. It looks like there is also a $K = 3^+$ band with a vibrational character. This complex situation is not represented in Fig. 22, and it is not further discussed, owing to the lack of experimental information.

In Fig. 24, the experimental gs band of the cross-conjugate nucleus ^{46}Ti is compared with SM predictions. Similarly to ^{44}Ti, the low spin states of the gs band seem to mix with two- and four-hole core configurations, even if at a reduced scale. In fact, if we lift up the SM values by about 400 keV to get the 8^+ levels close, we deduce that the 0^+, 2^+, and 4^+ levels are more bounded by about such value. Moreover, the yrare 0^+ level is calculated at 4280 keV while it is observed at 2611 keV. The experimental $B(E2)$ values for the yrast 2^+ and 4^+ levels are larger than predicted [56], owing to the relevant contribution of the two- and four-hole configurations, while the 6^+ level is essentially unaffected as it results from the level scheme.

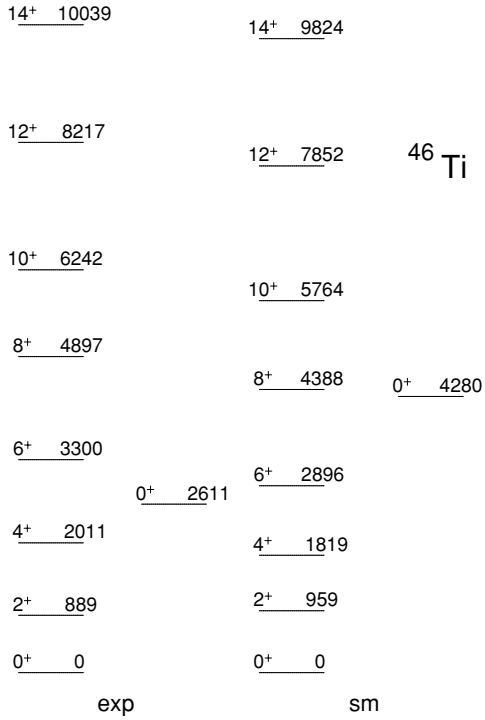

FIG. 24. Comparison of experimental gs band levels in ^{46}Ti with SM predictions.

In Fig. 25, the Q_s values in ^{50}Cr are compared with those in its cross-conjugate nucleus ^{46}Ti. The comparison is made neglecting the core contribution in the ^{46}Ti band. The estimated deformation of ^{46}Ti is smaller ($\beta^* \simeq 0.23$) than in ^{50}Cr but still relevant at low spins. In ^{46}Ti the change from the collective to the noncollective regime seems to occur in conjunction with the backbending at $I^\pi = 10^+$, similar to that at $I^\pi = 12^+$ in ^{48}Cr. The major difference is that it cannot be related simply to a termination in a seniority subspace. It seems that the change of regime does not necessarily start at a seniority subspace termination.

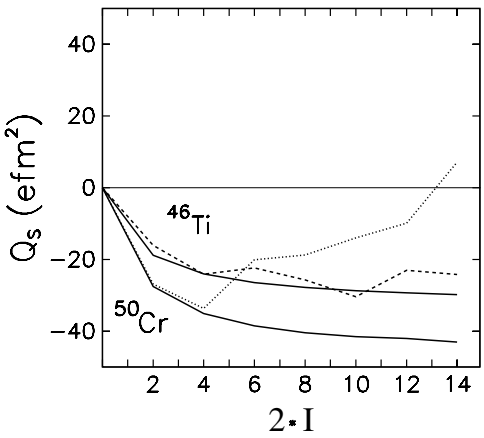

FIG. 25. Comparison between theoretical predictions for gs band Q_s values in ^{50}Cr and ^{46}Ti. Rotor values (solid lines) with $\beta^* = 0.28$ for ^{50}Cr and $\beta^* = 0.23$ for ^{46}Ti are compared with SM values (dotted and dashed lines, respectively).

IV. UNNATURAL PARITY BANDS

The shell-model description of unnatural parity bands requires the simultaneous consideration of two major shells and, implicitly, severe space truncations. Moreover, it is difficult to select a good effective interaction. In spite of these severe constraints, reasonable and even satisfactory agreement was achieved in several cases. It is too early for a detailed discussion, so only a brief summary will be presented, limited to odd-A nuclei.

In $N = Z + 1$ nuclei ^{45}Ti, ^{47}V, ^{49}Cr, and ^{51}Mn, low-lying $I^\pi = 3/2^+$ and $1/2^+$ levels were observed, which are interpreted as core-excited states having hole $[202]3/2^+$ and $[200]1/2^+$ Nilsson configurations, on which rotational bands are built. The heads of the $K^\pi = 3/2^+$ bands were identified at 293, 260, 1982, and 1817 keV, respectively, while the heads of the $K^\pi = 1/2^+$ band were at 1565, 1660, 2578, and 2276 keV, respectively. Such one-hole configurations in ^{45}Ti and ^{49}Cr are selectively populated in pickup reactions. The assignments in ^{47}V and ^{51}Mn are based on the decay scheme and the systematics.

SM calculations were performed mostly for the $K^\pi = 3/2^+$ band, and in this case the *pf* configuration space was enlarged to include a hole in the $1d_{3/2}$ orbital. These bands have generally a deformation different from that of the bond. The $K^\pi = 1/2^+$ band was observed long ago in ^{45}Ti [17], while that in ^{49}Cr only recently [18]. For their description with SM, the extension of the configuration space to include the $2s_{1/2}$ orbital was necessary. In fact, the $[200]1/2^+$ Nilsson orbital contains a large contribution from the spherical $2s_{1/2}$ orbital. The effective interaction, used in the calculations presented here, is that of Ref. [57] with some adjustment of binding energies.

The high-K bands predicted by SM at the lowest energy in such configuration space are $K^\pi = 9/2^+$, $11/2^+$, $13/2^+$, and $15/2^+$ in ^{45}Ti, ^{47}V, ^{49}Cr, and ^{51}Mn, respectively. They are produced by promoting a $[202]3/2^+$ nucleon to the first empty orbital and the recoupling of the three unpaired nucleons to the maximum K value, obviously with the necessary mixing of proton and neutron holes to satisfy isospin conservation. They can be also represented with the configurations $\pi d_{3/2}^{-1} \otimes {}^{46}\mathrm{V}(K = 3, T = 0)$, $\nu d_{3/2}^{-1} \otimes {}^{48}\mathrm{V}(K = 4, T = 1)$, $\pi d_{3/2}^{-1} \otimes {}^{50}\mathrm{Mn}(K = 5, T = 0)$ and $\nu d_{3/2}^{-1} \otimes {}^{52}\mathrm{Mn}(K = 6, T = 1)$, respectively.

The dipole band $K^\pi = 13/2^+$ in ^{49}Cr is yrast, and the observed first five members are well reproduced by SM calculation [15]. Its band termination is predicted at $33/2^+$. SM predictions are compared with experimental levels in Fig. 26, which is taken from Ref. [18]. Evidence was found of the $K^\pi = 7/2^+$ band, described also as a $\nu d_{3/2}^{-1} \otimes {}^{50}\mathrm{Mn}(I = 5, T = 0)$ configuration, but with an antiparallel coupling.

Members of the dipole band $K^\pi = 9/2^+ \pi d_{3/2}^{-1} \otimes {}^{46}\mathrm{V}$ $(K = 3, T = 0)$ in ^{45}Ti have been recently observed from $I^\pi = 17/2^+$ up to the termination at $I^\pi = 33/2^+$ [58]. The reason why members with spin values lower than $17/2^+$ are not observed may be that the 3^+ and 5^+ terms are rather close to the 7^+ level in ^{46}V, so that the decay-out is favored by the transition energy. The SS reflects that of the $K^\pi = 3^+$ band in ^{46}V [21], where it becomes larger approaching the band termination. This is probably the reason why dipole transitions and unfavored signature members were not observed both in the $K = 3$ band in ^{46}V and in the $K^\pi = 9/2^+$ band in ^{45}Ti. In Fig. 27, experimental levels are compared with SM predictions, taken also from Ref. [18].

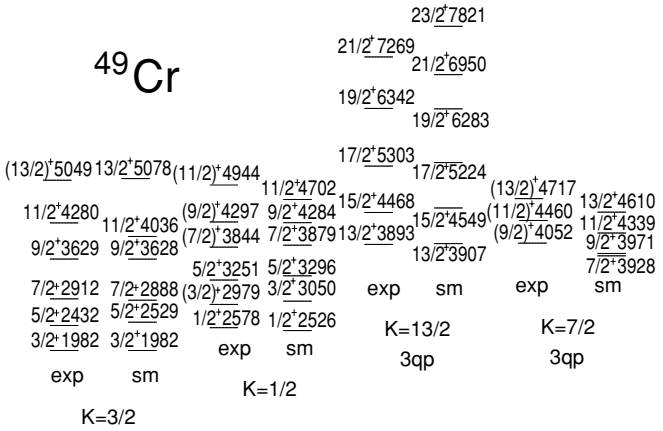

FIG. 26. Unnatural parity bands in ^{49}Cr.

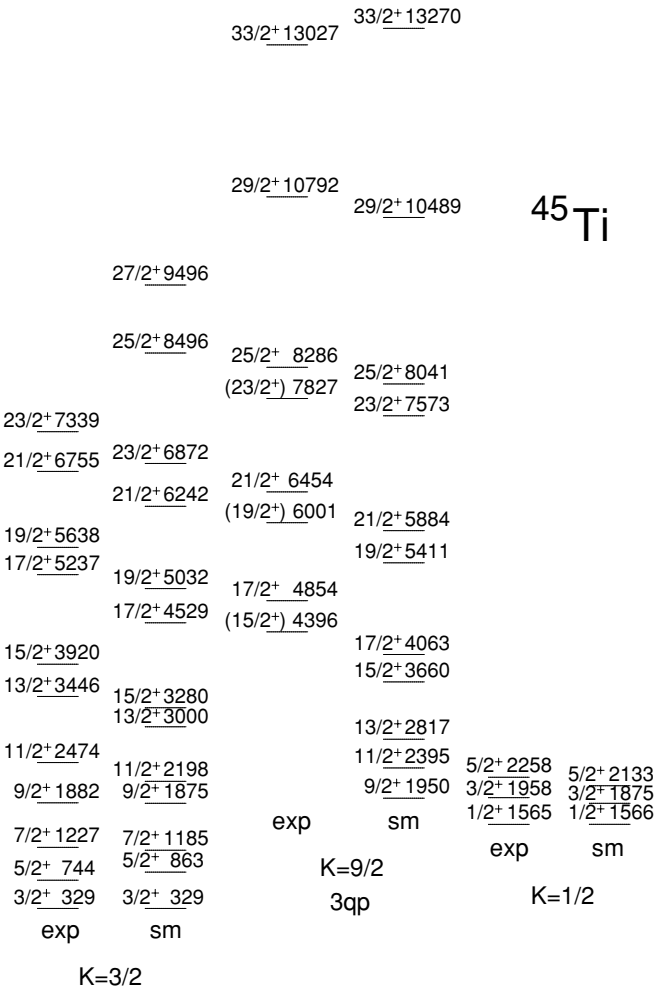

FIG. 27. Unnatural parity bands in ^{45}Ti.

Unfortunately, non-yrast structures are not known in ^{47}V, so the $K^\pi = 11/2^+$ band was also not observed.

In ^{51}Mn, the mentioned $K^\pi = 15/2^+$ band was also not observed. Instead, a positive parity band was recently observed up to $39/2^+$, which was attributed to the $\nu g_{9/2} \otimes {}^{50}\mathrm{Mn}(K = 5, T = 0)$ configuration [45]. This band is an intruder with respect to the so far considered configuration space, and its termination is $39/2^+$, in agreement with the observation. Since ^{50}Mn is prolate, the decoupled $[440]1/2^+$ intruder orbital should be considered. Assuming the coupling of the band $^{50}\mathrm{Mn}(K = 5, T = 0)$ with the $9/2^+$ state of the decoupled $1g_{9/2}$ band, one would expect a $19/2^+$ bandhead. Dipole transitions connecting the unfavored signature levels were not observed above $27/2^+$. This seems to reflect the fact that unfavored signature members were not observed in ^{50}Mn above $I = 9$, because of the large SS [59]. The predicted partner quadrupole band $\pi g_{9/2} \otimes {}^{50}\mathrm{Cr}(K = 0, T = 1)$ with $K^\pi = 9/2^+$ and termination at $I^\pi = 37/2^+$, is expected to be largely non-yrast.

The reason why the predicted "extruder" band $K^\pi = 15/2^+$ $\nu d_{3/2}^{-1} \otimes {}^{52}\mathrm{Mn}(K = 6, T = 1)$ was not observed so far is most likely the following. An estimate of its excitation energy is made considering that the isobaric analog state of the 6^+ gs level of ^{52}Mn in ^{52}Fe is at 5655 keV. Adding this value to the excitation energy of the yrast $3/2^+$ in ^{51}Mn of 1817 keV one gets 7472 keV for the $I^\pi = 15/2^+$ head, which is just lower than the $19/2^+$ head of the observed band. Its termination is predicted at $25/2^+$, well below that of the observed band at $39/2^+$, so the flux generated at high spin is efficiently captured by the intruder band, while little goes into the extruder one.

Large (τ, α) and (p, d) spectroscopic factor with $\ell_n = 0$ and $\ell_n = 2$ were observed in ^{53}Fe for the levels at 2967 and 3399 keV, respectively, so that they are identified as the $1/2^+$ and $3/2^+$ states containing a large fraction of the $2s_{1/2}$ and $1d_{3/2}$ orbitals, respectively, which appear to be inverted. Calculation made with the same interaction used for ^{49}Cr predict a slight inversion between the two levels, in tendential agreement with the experimental data.

As already mentioned, unnatural parity bands were also observed in several even-even and odd-odd nuclei, and they were described as having been obtained by lifting a nucleon from the $[202]3/2^+$ orbital to the *pf* space [57]. Satisfactory agreement was achieved in even-even ^{48}Cr, ^{50}Cr, and ^{46}Ti [7,48,56], as well as in odd-odd nuclei ^{46}V, ^{48}V [21,22].

V. CONCLUSIONS

Natural parity levels of several odd-*A* and even-even $N \simeq Z$ $1f_{7/2}$ nuclei are compared with SM predictions up to the spin termination in a $1f_{7/2}^n$ space.

Both experimentally and theoretically, levels can be organized in rotational bands at low spin, where band mixing of the order of 10% often occurs. The deformation decreases and the band mixing increases approaching the termination.

The prolate Nilsson diagram describes correctly the lowest sidebands in odd-A nuclei. Deformation alignment (strong coupling) appears to occur at low excitation energy in odd-*A* nuclei lying in the second half of the shell, while evidence of Coriolis decoupling is limited to nuclei in the first half of the shell.

SM calculations suggest the occurrence of γ bands in both $N = Z$ nuclei ^{48}Cr and ^{52}Fe. A signature for this is considered to be the large fragmentation of the wave functions. The experimental yrare 2^+ and 4^+ levels in ^{52}Fe and the (2^+) at 3632 and (3^+) at 4034 levels in ^{48}Cr are candidates for belonging to the γ bands.

The lowest 3-qp sidebands in ^{49}Cr and ^{51}Mn have $K^\pi = 13/2^-$ and $17/2^-$, respectively. They are described as being due to the excitation of one nucleon from the $[321]3/2^-$ to the $[312]5/2^-$ orbital and from the $[312]5/2^-$ to the $[303]7/2^-$ orbital, respectively. Only in the second case, a crossing with the gs band occurs, while the backbending of the ^{49}Cr gs band at $19/2^-$ is proposed to be related to the termination in the seniority $v = 3$ subspace. This conclusion shows that in general a backbending is not necessarily caused by band crossing and that the statement based on PSM calculations that backbendings in ^{49}Cr and ^{51}Mn are both caused by the crossing with a 3-qp $K^\pi = 7/2^-$ band [60] is untenable.

Similarly to ^{49}Cr the description of the backbending at 12^+ in ^{48}Cr cannot be achieved by standard deformed mean-field models. Experimental data and SM calculations exclude, in fact, a crossing of the ^{48}Cr gs band with a little deformed 4-qp $K = 2$ band, which served in the PSM analysis to explain the experimental backbending [13]. The Q_s curve points to a change of regime from collective rotational to nearly spherical at the backbending, in absence of any band crossing. What seems principally to occur is that with increasing spin the number of interacting particles in the $2p_{3/2}$ orbital decreases. Consequently the deformation induced by the quadrupole term also decreases. When the deformation becomes low enough, effects related to pairing become apparent, i.e., the backbending and the observed anomaly in the Q_s curve. Deformed mean-field theories cannot describe such effects, but they predict correctly the structure at the band termination.

The collective rotation of the gs band of the $N = Z + 1$ nuclei ^{47}V, ^{49}Cr, and ^{51}Mn is damaged above $I = 13/2$, indicating a change of regime.

The gs band levels of nuclei lying in the second half of the $1f_{7/2}$ shell, as ^{51}Mn, ^{51}Cr, ^{52}Fe and ^{53}Fe, become prolate non-collective ($\gamma = -120^\circ$) at the termination. Terminating states do not have pure $1f_{7/2}^n$ configurations as commonly believed; on the contrary, the large mixing with other orbitals of the *pf* configuration space increases the state deformation. These predictions agree essentially with those of CNS calculations.

The transitional levels between the initial collective rotation and the terminating regime present irregular features, as for instance a change of signature splitting, which are not yet understood in detail. It seems that the low number of valence nucleons does not allow a good collective motion.

A brief review is also presented for unnatural parity structures, whose SM description requires either core excitation of the *sd* shell or the intrusion of the $1g_{9/2}$ orbital.

The $1f_{7/2}$ region is a unique testing bench for the study of the origin of nuclear quadrupole deformation. There are more mechanisms of generating deformation, but what occurs in the $1f_{7/2}$ shell is a well understood case, where most

of the game is played by the orbitals $1f_{7/2}$ and $2p_{3/2}$. SM is a precise microscopic probe of any particle-alignment mechanisms, because it predicts accurate observables, which react to most structural effects, where other models may fail. Since SM provides very reliable values for the observables in the $1f_{7/2}$ shell, nuclear models based on the deformed mean-field approximation should calibrate their predictions on the SM ones. In particular, those models that assume a fixed deformation cannot be considered reliable in this region.

The general picture presented appears to be well grounded, but new experimental data are required, in particular to confirm the coexistence of rotational and vibrational degrees of freedom predicted by SM. Light-projectile-induced reactions appear to be the best chance for this purpose, since they would allow the accurate measurement of the properties of some important non-yrast levels of rather low spin.

ACKNOWLEDGMENTS

This theoretical survey follows a long experimental work performed at LNL. Discussions with coworkers, as well as the very stimulating ones with A. Zuker, are acknowledged.

[1] E. Caurier, A. P. Zuker, A. Poves, and G. Martinez–Pinedo, Phys. Rev. C **50**, 225 (1994).
[2] E. Caurier *et al*., Phys. Rev. Lett. **75**, 2466 (1995).
[3] G. Martinez-Pinedo, A. Poves, L. M. Robledo, E. Caurier, F. Novacki, and A. P. Zuker, Phys. Rev. C **54**, R2150 (1996).
[4] G. Martinez-Pinedo, A. P. Zuker, A. Poves, and E. Caurier, Phys. Rev. C **55**, 187 (1997).
[5] S. M. Lenzi *et al*., Z. Phys. A **354**, 117 (1996).
[6] S. M. Lenzi *et al*., Phys. Rev. C **56**, 1313 (1997).
[7] F. Brandolini *et al*., Nucl. Phys. **A642**, 387 (1998).
[8] F. Brandolini *et al*., in *Experimental Nuclear Physics in Europe*, *Seville, Spain, 1999*, edited by B. Rubio, M. Lozano, and W. Gelletly, AIP Conf. Proc. no. 495 (AIP, New York, 1999) p. 189.
[9] F. Brandolini *et al*., Phys. Rev. C **66**, 021302(R) (2002).
[10] S. M. Lenzi *et al*., Phys. Rev. Lett. **87**, 122501 (2001).
[11] T. Tanaka, K. Iwasawa, and F. Sakata, Phys. Rev. C **58**, 2765 (1998).
[12] A. Juodagalvis, I. Ragnarsson, and S. Åberg, Phys. Lett. **B477**, 66 (2000).
[13] K. Hara, Y. Sun, and T. Mizusaki, Phys. Rev. Lett. **83**, 1922 (1999).
[14] A. Juodagalvis and S. Åberg, Phys. Lett. **B428**, 227 (1998).
[15] F. Brandolini *et al*., Phys. Rev. C **60**, 041305(R) (1999).
[16] F. Brandolini *et al*., Nucl. Phys. **A693**, 517 (2001).
[17] J. Kasagi *et al*., Nucl. Phys. **A414**, 206 (1984).
[18] F. Brandolini *et al*., nucl-ex/0410037 (2004).
[19] E. Caurier, G. Martinez-Pinedo, F. Novacki, A. Poves, and A. P. Zuker, nucl-th/0402046 (2004).
[20] A. Poves, J. Sanchez-Solano, E. Caurier, and F. Novacki, Nucl. Phys. **A694**, 157 (2001).
[21] F. Brandolini *et al*., Phys. Rev. C **64**, 044307 (2001).
[22] F. Brandolini *et al*., Phys. Rev. C **66**, 024304 (2002).
[23] W. A. Richter, M. G. van der Merwe, R. E. Julies, and B. A. Brown, Nucl. Phys. **A523**, 325 (1991).
[24] S. Kahana, H. C. Lee, and C. K. Scott, Phys. Rev. **185**, 1378 (1969).
[25] T. Otsuka, M. Honma, and T. Mitsuzaki, Phys. Rev. Lett. **81**, 1588 (1998).
[26] M. Honma, T. Otsuka, B. A. Brown, and T. Mizusaki, Phys. Rev. C **69**, 034335 (2004).
[27] M. Hasegawa, K. Kaneko, and S. Tazaki, Nucl. Phys. **A674**, 411 (1999); **A688**, 765 (2000).
[28] M. Dufour and A. Zuker, Phys. Rev. C **54**, 1641 (1996).
[29] E. Caurier, Shell Model code ANTOINE, IRES, Strasbourg 1989–2002.
[30] E. Caurier and F. Novacki, Acta Phys. Pol. **30**, 705 (1999).
[31] A. Zuker, J. Retamosa, A. Poves, and E. Caurier, Phys. Rev. C **52**, R1741 (1995).
[32] A. Bohr and B. R. Mottelson, in *Nuclear Structure* (Benjamin, New York, 1975) Vol. 2, p. 45.
[33] K. E. G. Löbner, M. Vetter, and V. Hönig, Nuclear Data Tables **7**, 495 (1970).
[34] S. E. Larson, G. Leander, and I. Ragnarsson, Nucl. Phys. **A307**, 189 (1978).
[35] S. J. Williams *et al*., Phys. Rev. C **68**, 011301(R) (2003).
[36] W. J. Gerace and A. M. Green, Nucl. Phys. **113**, 641 (1968).
[37] J. M. Espino *et al*., LNL-INFN (REP)-182/2002, p. 10 (unpublished).
[38] I. Ragnarsson, V. P. Jansen, D. B. Fossan, N. C. Schmeing, and R. Wadsworth, Phys. Rev. Lett. **74**, 3935 (1995).
[39] B. G. Dong and H. C. Guo, Eur. Phys. J. A **17**, 25 (2003).
[40] S. Åberg, Nucl. Phys. **A306**, 89 (1978).
[41] J. A. Sheikh, D. D. Warner, and P. van Isacker, Phys. Lett. **B443**, 16 (1998).
[42] C. A. Ur *et al*., Phys. Rev. C **58**, 3163 (1998).
[43] J. A. Cameron *et al*., Phys. Rev. C **58**, 808 (1998).
[44] B. Bengtsson and S. Frauendorf, Nucl. Phys. **327**, 139 (1979).
[45] J. Ekman *et al*., Phys. Rev. C **70**, 014306 (2004).
[46] J. Ekman *et al*., Eur. Phys. J. A **9**, 13 (2000).
[47] M. A. Bentley *et al*., Phys. Rev. C **62**, 051303(R) (2000).
[48] F. Brandolini, Eur. Phys. J. A **20**, 139 (2004).
[49] J. A. Cameron *et al*., Phys. Rev. C **49**, 1347 (1994).
[50] K. Jessen *et al*., Phys. Rev. C **68**, 047302 (2003).
[51] C. A. Ur, Eur. Phys. J. A **20**, 113 (2004).
[52] A. Poves and G. Martinez-Pinedo, Phys. Lett. **B430**, 203 (1998).
[53] C. Rusu *et al*., Phys. Rev. C **69**, 024307 (2004).
[54] C. D. O'Leary *et al*., Phys. Rev. C **61**, 064314 (2000).
[55] A. Willis *et al*., Nucl. Phys. **A499**, 367 (1989).
[56] F. Brandolini *et al*., Phys. Rev. C **70**, 034302 (2004).
[57] A. Poves and J. Sanchez-Solano, Phys. Rev. C **58**, 179 (1998).
[58] P. Bednarczyk *et al*., Eur. Phys. J. A **20**, 45 (2004).
[59] C. E. Svensson *et al*., Phys. Rev. C **58**, R2621 (1998).
[60] V. Velasquez, J. G. Hirsch, and Y. Sun, Nucl. Phys. **A686**, 129 (2001).